AN ABSTRACT OF THE THESIS OF

Erick McAdam for the degree of Master of Science in Sustainable Forest Management presented on December 7, 2015.

Title: Using Remote Sensing and Process-based Growth Modeling to Predict Forest Productivity Across Western Oregon

Abstract approved: _____

Thomas Hilker

Accurate measurement of forest productivity is fundamental to understand the carbon balance of forested ecosystems. Recent changes in climate highlight the importance of developing methods to measure forest productivity so that sound economic and environmental decision can be made. Efforts to measure forest productivity across the landscape using remote sensing suffer from limitations inherent in individual sensors. We combine approaches to estimate forest productivity on Douglas-fir plantations using optical passive remote sensing to estimate stand ages, single-pass LiDAR sampling to estimate structural properties, and a process-based growth model (3PG) to assess variation in soil properties across western Oregon. Our results indicate that it is possible to estimate both

site index and difficult-to-obtain soil properties across the landscape using two types of remote sensing instruments in combination with modeling. While we believe that the approach is sound, we found that the quality of extrapolated climatic data very much affects the derived values of soil properties assessed by modeling. In contrast, estimates of maximum leaf area index with LiDAR proved a reliable independent means to assess site productivity because plantations reach maximum values in less than two decades after establishment.

Using Remote Sensing and Process-based Growth Modeling to Predict Forest Productivity across Western Oregon

by

Erick McAdam

A THESIS

submitted to

Oregon State University

in partial fulfillment of
the requirements for the
degree of

Master of Science

Presented December 7, 2015
Commencement June 2016

Master of Science thesis of Erick McAdam presented on December 7, 2015

APPROVED:

Major Professor, representing Sustainable Forest Management

Head of the Department of Forest Engineering, Resources, and Management

---

Dean of the Graduate School

I understand that my thesis will become part of the permanent collection of Oregon State University libraries. My signature below authorizes release of my thesis to any reader upon request.

Erick McAdam, Author

ACKNOWLEDGEMENTS

I would like to thank my primary adviser, Thomas Hilker, for his moral and economic support, patience, and always being available when I needed help. Thanks to Hailemariam Temesgen for his generosity in providing much needed funds during the last several months at Oregon State University. I would also like to give special thanks to Richard Waring for his guidance, sharing his knowledge, pushing me to do more model runs, and his constant encouragement throughout this process. Also, many thanks to all my committee members for being so accommodating and for their helpful advice. To all my friends in Corvallis for always being there to distract me. My time in Oregon would not have been as enjoyable without you. Lastly, I would like to express my gratitude to my family for their continued support throughout my stay in Oregon.

TABLE OF CONTENTS

Page

Introduction ……1

Literature Review ……4

Materials and Methods ……10

Study area ……10

Landsat disturbance and stand age estimation ……10

Estimates of site growth potential using site index ……12

Climate data ……14

LiDAR data ……19

Growth modeling ……20

Model parameterization ……22

Results ……24

Discussion ……32

Conclusion ……37

Literature cited ……39

Appendix ……46

LIST OF FIGURES

Figure Page

1. Map of western Oregon showing site classes and approximate stand locations (red dots) ……13

2. Map of total annual precipitation for western Oregon showing stand locations as red spots……..15

3. Map of mean daily short wave radiation for western Oregon showing stand locations as red spots.....16

4. Map of mean annual maximum temperatures for western Oregon showing stand locations as blue spots ……17

5. Map of mean annual minimum temperatures for western Oregon showing stand locations as blue spots……18

6. Visualization of surface normalized LiDAR point cloud of different forest in our sampling area……24

7. Landsat-derived map of perceived disturbances from 1983-2012 in western Oregon ……26

8. Number of recorded 30x30m disturbances by year in the state of Oregon……..27

9. Relationship between 3PG modeled v. LiDAR- derived estimates of LA ……28

10. Derived age-height relationship for 111 stands sampled ……..30

11. Derived soil fertility rankings (FR) from inverting the 3-PG model while assuming that the available soil water storage capacity was fixed at 300mm and that stand leaf area index (LAI) was equivalent to that estimated by LIDAR……31

12. A Observed LiDAR LAI plotted against estimated stand age using McArdle *et al.*, (1949) lower to upper height limits for each site class……..32

13. Site index classification in western Oregon using McArdle *et al.*, (1949) yield tables …….35

14. LiDAR LAI v age using the lower limit of the next higher site class height category as the upper limit of the lower site class……..36

LIST OF TABLES

Table Page

1. McArdle *et al.*, (1949) site index at 50 years height ranges (meters)……12

2. LiDAR information for each DOGAMI delivery corresponding to stand locations……..19

3. 3-PG Model Parameters ……23

4. Forest Stand Sampling Statistics ……..29

LIST OF APPENDIX FIGURES

Figure Page

A1. Differences in mean annual precipitation (mm) projected by ClimateWNA in comparison to the PRISM model.....46

A2. Range in PRISM maximum and minimum temperatures across western Oregon for the months of April to September.....47

A3. ClimateWNA maximum and minimum temperature ranges for the months of April to September across western Oregon.....48

INTRODUCTION

Net primary productivity is considered an important indicator of ecosystem health and an essential component in understanding the global carbon cycle (Pan et al., 2014). Because of its importance in evaluating ecosystem function and the urgency to understand how ecosystems will react to global climate change, there has been increased interest in finding ways to accurately measure and predict NPP at different temporal and spatial scales (Field, Randerson, & Malmström, 1995a; Goetz et al., 1999; Nemani et al., 2003; Randerson, Chapin, Harden, Neff, & Harmon, 2002). Changes in the rates of projected height growth and in the amount of foliage accumulated by vegetation are two measures that are worth investigating.

One of the main limitations researchers face when monitoring NPP is the paucity in repeated measurements necessary to accurately estimate it. Traditional methods of monitoring terrestrial primary production have relied either on inventory plots or on growth curves derived from ground-based measurement of tree heights, which are later used to create growth and yield tables, and to classify areas with different growth potentials (Skovsgaard & Vanclay, 2008). Although these methods are considered to be accurate, they require continuous measurement over long periods, making them difficult to implement over large areas as well as costly. Also, because they make use of statistical relations to convert specific tree measurements to volumes and total biomass, traditional approaches describe a site's growth potential rather than actual growth unless tree densities and ages are recorded. Even then, the assumption of a stable environment may be invalid under intense management practices and a changing climate.

Recent developments in remote sensing allow researchers to address some of the challenges associated with the need to make repeated measurements of tree height, stand wood volume and leaf

area density. For more than four decades, satellite-borne sensors have used the sun's energy to provide a reflected spectral image from which land-cover types and disturbances can be mapped (Landgrebe, 1997). These passive sensors are unable, however, to penetrate dense vegetation. To accomplish the latter requires pulsed energy generated from light-emitted lasers (Light Detection and Ranging - LiDAR) (Wulder, Bater, Coops, Hilker, & White, 2008) or from long-wave radio waves (RADAR) (Imhoff, Story, Vermillion, Khan, & Polcyn, 1986). Although LiDAR is not yet available from satellite-borne instruments with adequate resolution, aircraft –mounted instruments provide the appropriate resolution where coverage is available for both tree heights and leaf area density.

In addition to height measurements from remote sensing, modeling approaches have provided new insights into forest growth and the factors limiting it at a given time. If uniformly-aged forests grow at locations where the environmental conditions are well known, it is possible to use process-based models to estimate growth at regular intervals (Weiskittel, Hann, Kershaw, & Vanclay, 2011). Because physiological processes are directly affected by climate and soil properties, process models can identify the relative importance of different climatic variables, as well as soil properties affecting the storage of water and nutrients. Oftentimes parameterization of such models is, however, challenging as traditional inventory based observations cannot provide vegetation parameters in spatially continuous fashion across the landscape.

To overcome some of the limitations in estimating vegetation growth, this thesis combines estimates of height and vegetation cover obtained from remote sensing with the insights provided from a process-based growth model in a study of more than 100 plantations of Douglas-fir scattered over much of western Oregon. While we believe our efforts represent an improvement over conventional methods, we are aware that repeated coverage and reliable meteorological data are essential to advance the approach. To compensate for the lack of repeated measurements we established a

chronological sequence of different aged Douglas-fir plantations. In doing this, we made a number of assumptions: (1) that we were able to classify each stand correctly according to its site index, (2) that extrapolated climatic data provides a reliable estimates of monthly averaged precipitation, incident solar radiation, and temperature extremes,. 3) that the date of stand establishment following harvesting was correctly identified, 4) that estimates of leaf area density and stand heights were accurately measured, and (5) that stands were not thinned or otherwise manipulated since their establishment. We simplified our analysis by also assuming that climatic conditions have remained stable for the short period over which we collected data on plantation growth (27 years).

LITERATURE REVIEW AND BACKGROUND

Forests cover more than one third of the global land area and are important for climate regulation and carbon sequestration (FAO, 2015; Muning et al., 2011). There is uncertainty of how changing climate will affect forest productivity, which is directly linked to biomass production and carbon storage (Kohl et al., 2015). Understanding the mechanisms by which forests interact with the atmosphere to produce biomass, and therefore the influence that forest have on the earth's energy and water balance are important if we are to predict future climate scenarios (Randerson et al 2002; Steffer, Nobel, & Canadell, 1998). Recent changes in climatic conditions highlight the value of developing accurate models to account for gains and losses in carbon storage by forests (Law & Waring, 2015). Likewise, knowing the current state of carbon storage and understanding the components of carbon fluxes creates a baseline against which foresters and decision makers can compare policies that are designed to be both economically and ecologically sound (Gibbs, Brown, Niles, & Foley, 2007) .

The total carbon balance of forests can be separated into carbon uptake (or gross primary productivity, GPP) and carbon loss through plant and soil respiration. The difference between GPP and plant respiration is net primary productivity (NPP), an estimate of annual net accumulation of biomass, above and below-ground. Above-ground tree biomass can be estimated by periodically measuring stem diameter and height growth on inventory plots, and using measurement and allometric equations to convert dimensional measurements to volume and mass. Accounting for below-ground biomass in roots and leaf turnover rates is much harder. A disturbance by fire, erosion, or removal of plant material can cause the carbon balance of an ecosystem to go negative (Kira & Shidei, 1967). Although empirical stem growth models based on biometric analyses are commonly used in forestry, these rarely consider the effect of different management practices and climate on growth (Battaglia & Sands, 1998; Constable & Friend, 2000).

More recently, Light Detection and Ranging (LiDAR), a remote sensing technique were pulsed laser light is reflected off of tree canopies and the ground, has been used as an inventory tool to measure attributes of forests that are of interests to managers (Korhonen, Korpela, Heiskanen, & Maltamo, 2011; Lim, Treitz, Wulder, St-Onge, & Flood, 2003; van Leeuwen & Nieuwenhuis, 2010; Wulder et al., 2012) . LiDAR facilitates measurements of the three-dimensional distribution of vegetation components and sub-canopy architecture, thereby providing high spatial resolution topographic elevation data, and accurate estimates of vegetation height, cover density, and other aspects of canopy structure (Hilker et al., 2008; Lefsky et al., 2005). Measurement errors for individual tree heights (of a given species) are typically in the order of less than 1.0 m (Persson, Holmgren, & Söderman, 2002) and less than 0.5 m for plot-based estimates of maximum and mean canopy height with full canopy closure(Naesset & Okland, 2002). LiDAR systems can be classified into discrete return and full waveform sampling systems. Full waveform LiDAR systems compensate for a coarse spatial resolution (10 – 100 m) with a finer, and fully digitized, vertical resolution, providing full sub-meter vertical profile (Coops et al., 2007). Discrete return systems on the other hand typically record only up to five returns per laser footprint (Lim et al., 2003) at a footprint size of about 0.2m (Coops et al., 2007). These systems are optimized for the derivation of sub-meter accuracy terrain surface heights (Schenk, Seo, & Csatho, 2001).

LiDAR's advantage over passive remote sensing techniques lays in its ability to penetrate dense forest canopies and to give accurate estimates of tree heights, canopy leaf area and volume, as well as variations in micro-topography over large areas (Coops et al., 2007; Magnussen & Boudewyn, 1998; Naesset, 1997; Xiaoye Liu, 2008). However, using LiDAR alone to measure above-ground growth requires repeated observations (Dubayah et al., 2010). Repeated surveys with LiDAR are uncommon because

currently, suitable sensors are only designed to be flown on fixed winged aircraft. Once suitable satellite-borne LiDAR is available, data from repeat surveys will be much easier to acquire (REF).

Because of the paucity of repeat measurements, even on the ground, foresters often describe growth potential instead of actual stand growth to characterize site quality and to avoid the need for repeated measurements. One common measure of potential productivity is site index (SI) which classifies forest land into growth categories based on the average total height of dominant and co-dominant trees, typically referenced to age 50 or 100. In Oregon, a five-class system is commonly used, with site 1 (S1) represented the highest and site 5 (S5) the lowest category (Mcardle, Meyer, & Bruce, 1949). SI incorporates all the environmental factors that affect growth but does not distinguish the constraints imposed by any single variable. While a valuable and widely applied method, site index may not predict actual growth rates for a variety of reasons (Skovsgaard & Vanclay, 2008). First of all, site index is assumed to be invariable over time, which assumes no change in soil properties, climate conditions or management practices (Monserud & Rehfeldt, 1990; Monserud et al., 2008; Valentine, 1997). Also, SI classification requires the presence of identifiable tree species of similar ages that have grown without overhead competition or injury throughout their lives (Ford & Bassow, 1989). Changes in SI can go unnoticed unless frequent assessments are made. Lastly, forest inventory observations are typically spatially discrete, scaling across the landscape presents additional challenges.

As an alternative to site indices, stand growth can also be estimated using process-based growth models. Such models make growth predictions based on detailed knowledge of environmental factors and physiological processes that include light interception by the canopy, photosynthesis, leaf stomatal responses, respiration, carbon allocation, leaf turnover, soil water and nutrient dynamics (Weiskittel et al., 2011). Process-based growth models have the potential to estimate productivity in areas where forests are absent, and to quantify the effect of disease and drought. For these reasons, process-based

models have gained popularity in recent years (Almeida et al., 2004; Constable & Friend, 2000). However, testing the validity of process-based models requires a much larger set of measurements than those required to validate SI (Battaglia & Sands, 1998). When extrapolating across landscapes, reliable climatic and soils data are particularly difficult to obtain, limiting the use of process-based growth models in many situations.

Efforts to parameterize growth models across the landscape using passive optical remote sensing often rely on satellite derived estimates of incident photosynthetically active radiation (PAR), the fraction of PAR absorbed by the forest canopy (f_{APAR}), precipitation and temperature (Coops & Waring, 2001a, 2001b; Goetz et al., 1999; Powell et al., 2010). Some of the main limitations with this approach are well known problems associated with passive optical remote sensing, namely instrument saturation at high leaf area index (LAI) (McLeod & Running, 1988; Franklin et al., 1997), coarse spatial resolution (Powell et al., 2010), and inaccuracy in extracting forest attributes (Waring, Coops, & Landsberg, 2010).

While single method forest growth estimation has many advantages, there are also significant limitations associated with each approach. More recently, researchers have favored a multiple method approach to forest growth estimation taking advantage of the strengths of each approach while minimizing their limitations (Field, Randerson, & Malmström, 1995b; Moran, Maas, & Pinter, 1995). LiDAR has been used as a complement for other forms of passive optical remote sensing and process-process based growth modeling because it is able to accurately measure the vertical structure of forest canopies. While it is possible to extract forest height from optical passive remote sensors, LiDAR offers independent validation of forest attributes such as stand height and leaf area index (LAI) useful for the estimation of forest productivity and biomass estimation (Koetz et al., 2007).

Previous attempts to estimate growth using the multiple method approach have used a combination of satellite optical remote sensing, full waveform LIDAR, and process-based growth models

(M.A. Lefsky, Turner, Guzy, & Cohen, 2005). While this approach allows for increased spatial coverage, provided that LiDAR coverage is available throughout the region of interest, model parameterization is independent of the remotely sensed data. Instead, temporally separated LiDAR surveys are used to estimate periodic increases in above ground biomass which are later compared to the growth model predictions. However, the large footprint size of the waveform LiDAR instrument (5-10 meters) may be too coarse to correctly estimate tree-level biomass and other attributes necessary for accurate growth estimation at different spatial scales (Popescu, Wynne, & Nelson, 2003). Similarly, statistical techniques have been used to aid in the parameterization of process-based growth models across areas where little or no data is available. This approach combines a tree-level forest growth model (Forest Vegetation Simulator (FVS)), ground measurement of forest attributes, and nearest neighbor imputation (kNN) to create "virtual" forest inventories from which growth projections can be made (kNN)(Falkowski et al., 2010). Härkonën *et al.*, (2013) approached the problem of growth estimation using airborne LiDAR, a simplified process-based growth model, and climate data to predict growth Scots Pine plots in Finland. While the quality of the LiDAR data they used was low, the growth model parameterized using LiDAR derived forest attributes performed better than well-known empirical growth models, and underperformed as compared to growth predictions of the same process-based model parameterized using ground data. The predictions of the LiDAR-parameterized growth model in this study were contingent on the correct soil fertility parameters and LAI estimation. While LiDAR LAI estimates are relatively easy to obtain reasonably good even without ground validation (Korhonen et al., 2011) soil properties are difficult to obtain at the spatial scale required for appropriate process-based model growth predictions (Coops, Waring, & Hilker, 2012)

More recent methods of growth estimation use the multiple method approach involve Landsat forest disturbance detection to estimate stand ages, IKONOS stereo imagery in combination with airborne LiDAR to estimate forest stand heights, and Forest Inventory and Analysis National Program

ground data to develop regression predictions of above ground biomass as a function of LiDAR first returns (Neigh et al., 2016). While this approach may produce estimates of growth across large areas, it only measures the difference between two points in time and may not be useful in making predictions of growth over time.

MATERIALS AND METHODS

Study area

Western Oregon is characterized by two major mountain ranges separated by an extensive valley system. Outside the valley system the majority of the area is covered by coniferous forests dominated in large part by successional and old growth Douglas-fir forests which vary in productivity from 3 to 35 Mg ha^{-1} $year^{-1}$ (Jarvis & Leverenz, 1983) . The climate of the region varies greatly but is characterized by wet, mild winters and warm, dry summers. Mean monthly minimum temperatures range from -5°C in the high Cascade Mountains to 5°C in the coastal areas, whereas mean maximum temperatures range from 20°C along the Oregon coast to 30°C in the southern parts of the region. Total annual precipitation is highly variable across the region with the lowest values recorded in the southern portion (500mm $year^{-1}$) and up to 5000mm $year^{-1}$ in some coastal regions and higher elevations in the Cascades (Franklin & Dyrness, 1988). Of the more than 12 million hectares of forested land in Oregon, more than 60% are publically owned. Commercial timber companies own about 2.4 million hectares of forestland in Oregon, while thousands of small private owners account for some 1.9 million more. The U.S. Department of Agriculture's Forest Service (5.8 million hectares) and the U.S. Department of the Interior's Bureau of Land Management (1.5 million hectares) are by far the largest managers of Oregon's public forestlands. Typical rotation for managed forests is between 30-40 years but varies by ownership (http://oregonforests.org/sites/default/files/publications/pdf/Federal_Forestlands.pdf).

Landsat Disturbance Index and Stand age estimation

Landsat Thematic Mapper (TM) data for this project were acquired from USGS Earth Resources Observation and Science (EROS) Center Science Processing Architecture (ESPA)

(https://espa.cr.usgs.gov) spanning observations from 1983-2012 (path 46, rows 28-31). The images were stacked according to path/row and later merged into monthly mosaic composites of the best available pixels. All images were atmospherically corrected using the LEDAPS algorithm (Masek et al., 2013) . LEDAPS (Landsat Ecosystem Disturbance Adaptive Processing System) processes Landsat imagery to surface reflectance, using atmospheric correction routines developed for the Terra MODIS instrument (Vermote et al., 1997). The algorithm provides calibration, TOA reflectance, cloud masking, and an atmospheric correction preprocessing chain. This atmospheric correction incorporates routines previously applied to the Terra MODIS instrument. Additional cloud screening was performed using fmask (Zhu & Woodcock, 2012). Finally, images were composited for each year using best available pixels observed between June and September of each year. This period was chosen to minimize seasonal changes in composited images and to allow change detection on an annual basis.

Stand ages for most of the managed forested area were estimated from the 30 year Landsat archive, by assuming that the date of a recorded disturbance was close to the date of reforestation (as is required by law in the Oregon Forest Practices Act). We estimated stand level disturbances using Healy's et al. (2005) disturbance index (DI). This index is a transformation of the Tasseled Cap algorithm calculated using three variables (brightness, greenness and wetness) from Landsat TM/ETM+ data. Disturbance was quantified as the normalized spectral distance of any given pixel from a nominal "mature forest" class and is usually an indication of a clear cut leading to stand replacement. The perceived date of disturbance was mapped at 30m resolution at yearly intervals over the entire study area.

Estimates of site growth potential using Site index and stand selection

Stands were selected in regions where LiDAR coverage and detected disturbances within the past 30 years overlapped. In order to estimate stand age, only detected disturbances as a result of harvests (clear cuts) were considered. Ortho-rectified aerial images were used to as used to assess stand height homogeneity and to exclude stand where detected disturbance were likely the result of recent fire. Areas designated by a single disturbance date were considered the origin of a new plantation and therefore a stand. Adjacent areas separated by 100 m or less where the year of disturbance was the same were considered a single stand. Using a map of site index at 50 years from Latta, Temesgen, & Barrett (2009) we assigned each forest stand to one of 5 different site index regions in western Oregon using McArdle, Meyer, & Bruce (1949) site index classification (Table 1) (Figure 1).

Table 1. McArdle *et al.*, (1949) site index at 50 years height ranges (meters). Site index 1 (S1) represents the best site while site index 5 (S5) the worst.

	S1	S2	S3	S4	S5
Lower Limit	40	34	28	21	<17
Upper Limit	>40	38	32	26	19

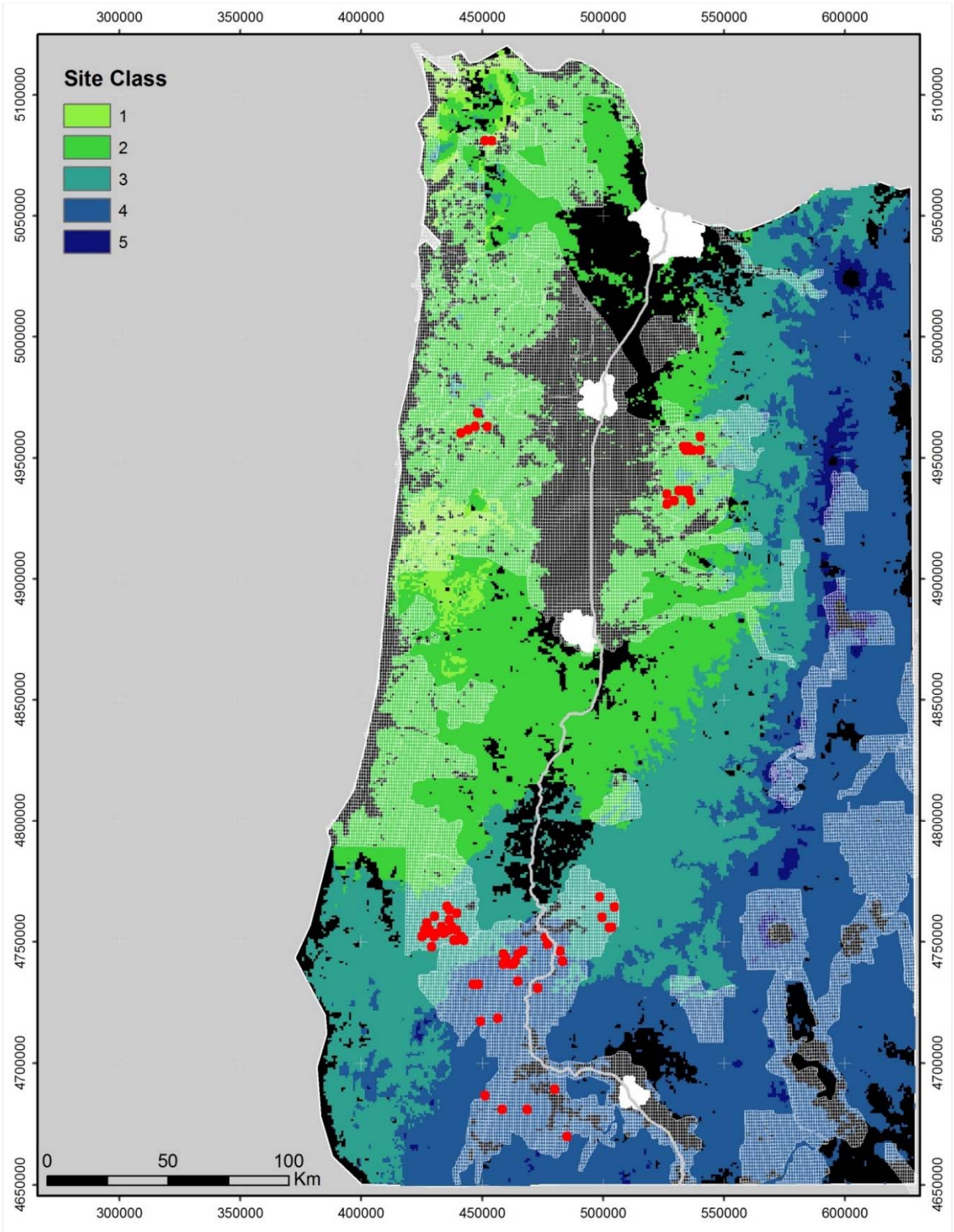

Figure1. Map of western Oregon showing site classes and approximate stand locations (red dots). Grey shaded areas represent current LiDAR coverage for the state of Oregon available through DOGAMI (http://www.oregongeology.org/sub/projects/olc/).

Climate data

Long-term weather observations (1981-2010) across the region were obtained from Climate-WNA (Western North America) (http:// http://cfcg.forestry.ubc.ca/projects/climate-data/climatebcwna/#ClimateWNA). Climate-WNA is based on the Parameter-elevation Regressions on Independent Slopes Model (PRISM), which accounts for variations in precipitation and temperature associated with mountainous terrain through interpolation of a digital terrain model described by Wang *et al.* (2012). ClimateWNA outputs climate layers at 1 Km resolution (Figure 2-5).

Mean monthly daytime vapor pressure deficits (VPDs) were estimated by assuming that the saturated water vapor during the day would be equivalent to that held at the monthly mean minimum temperature (Kimball, Running, & Nemani, 1997). The maximum mean VPD was calculated each month as the difference between the saturated vapor pressure at the mean maximum and minimum temperatures. Mean daytime VPD was calculated at two thirds of the maximum value. The number of days per month with subfreezing temperatures (≤2 °C) was estimated from empirical equations with mean minimum temperature. Monthly estimates of total incoming short-wave radiation were obtained by combining the synoptic and zonal variation captured by the North American Regional Re-Analysis (NARR) with topographically-driven variation based on Fu and Rich (2002), similar to the approach applied by Schroeder *et al* (2009).

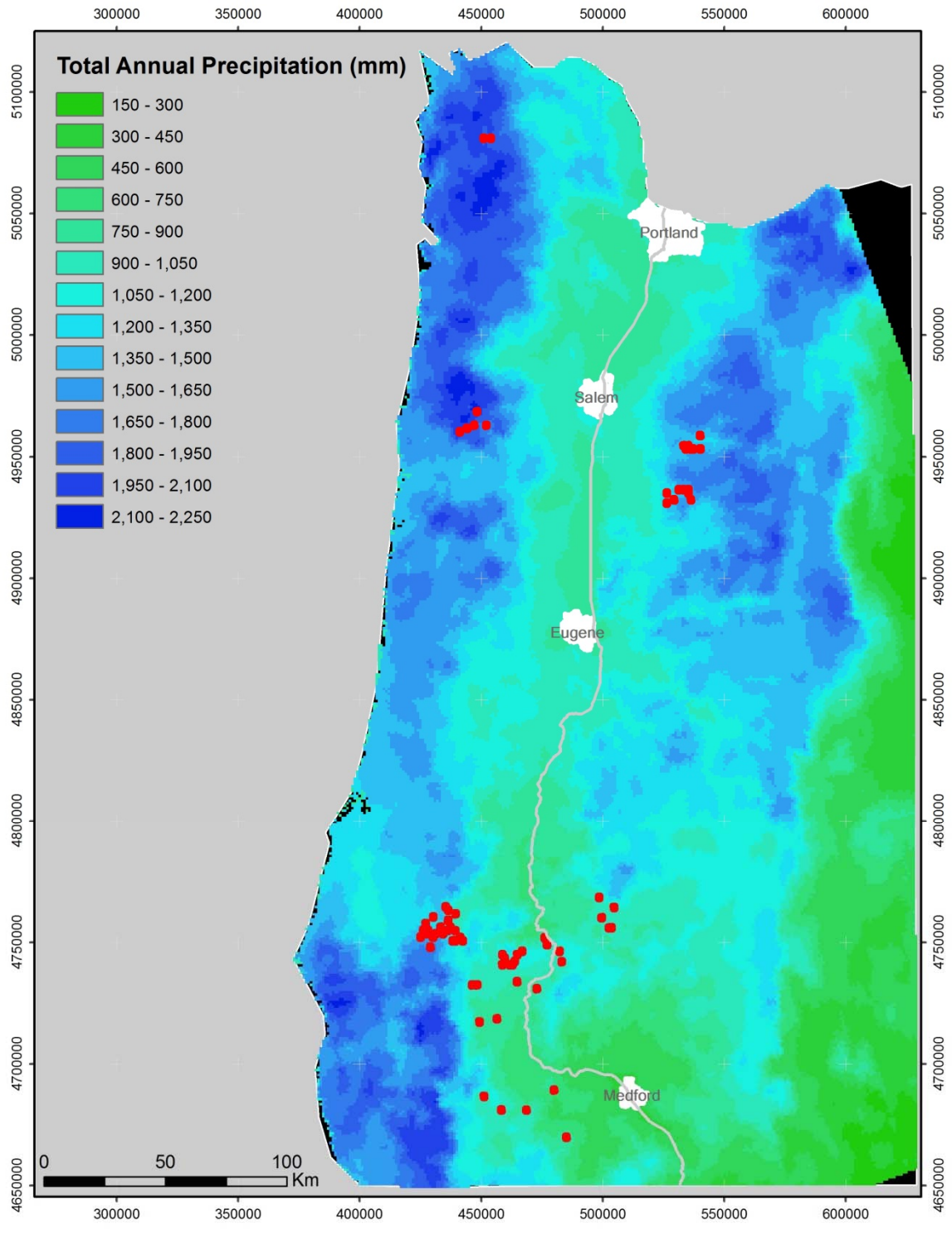

Figure 2. Map of total annual precipitation for western Oregon showing stand locations as red spots.

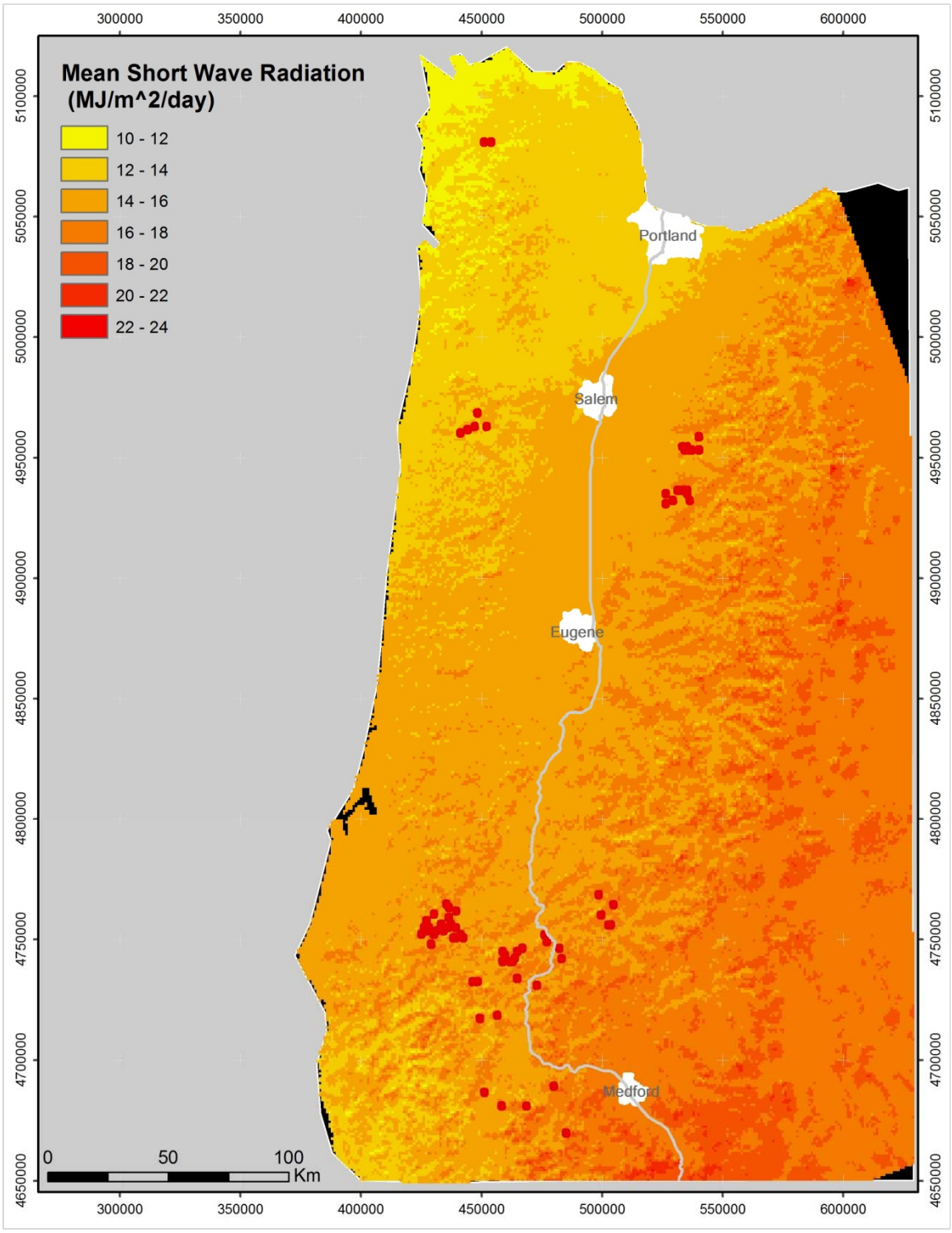

Figure3. Map of mean daily short wave radiation for western Oregon showing stand locations as red spots.

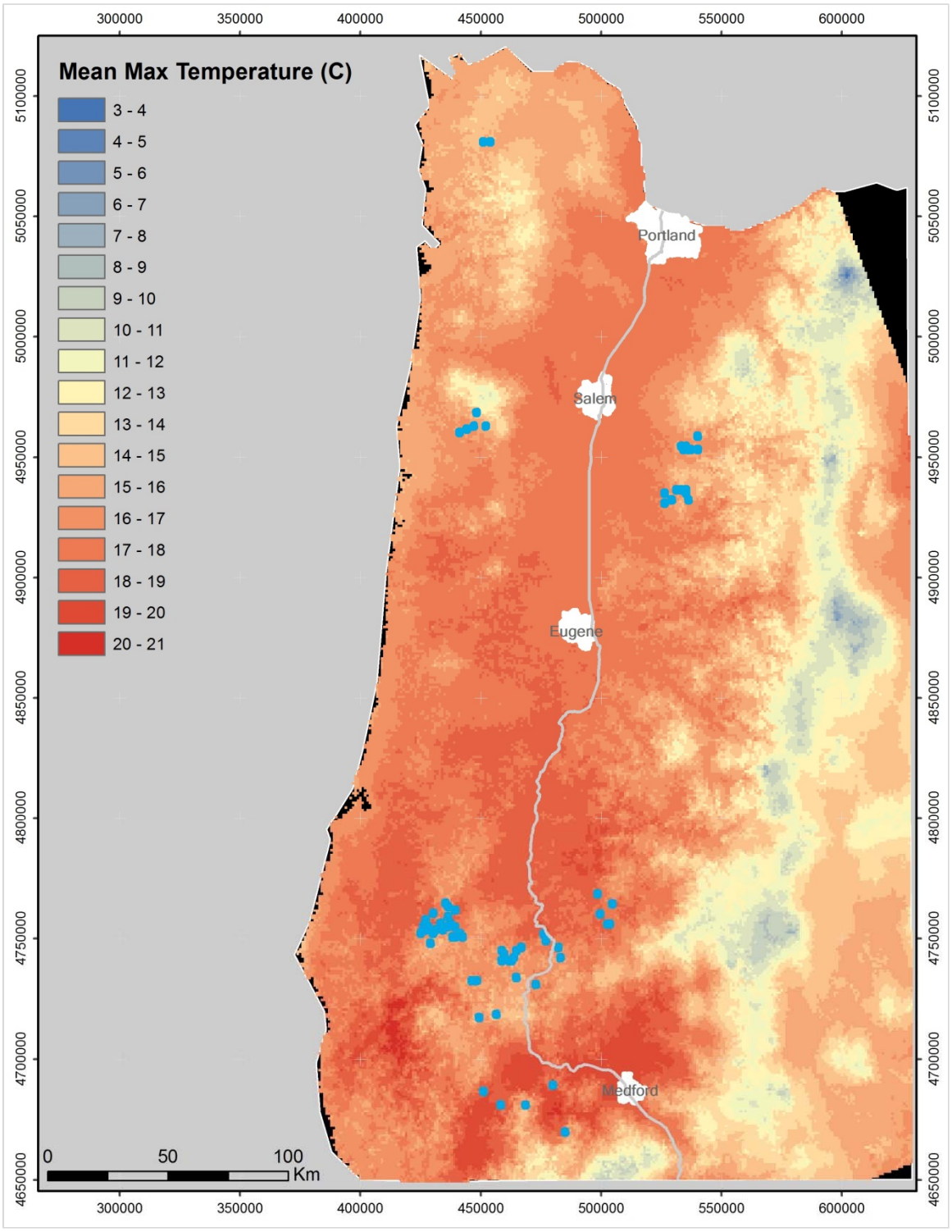

Figure4. Map of mean annual maximum temperatures for western Oregon showing stand locations as blue spots

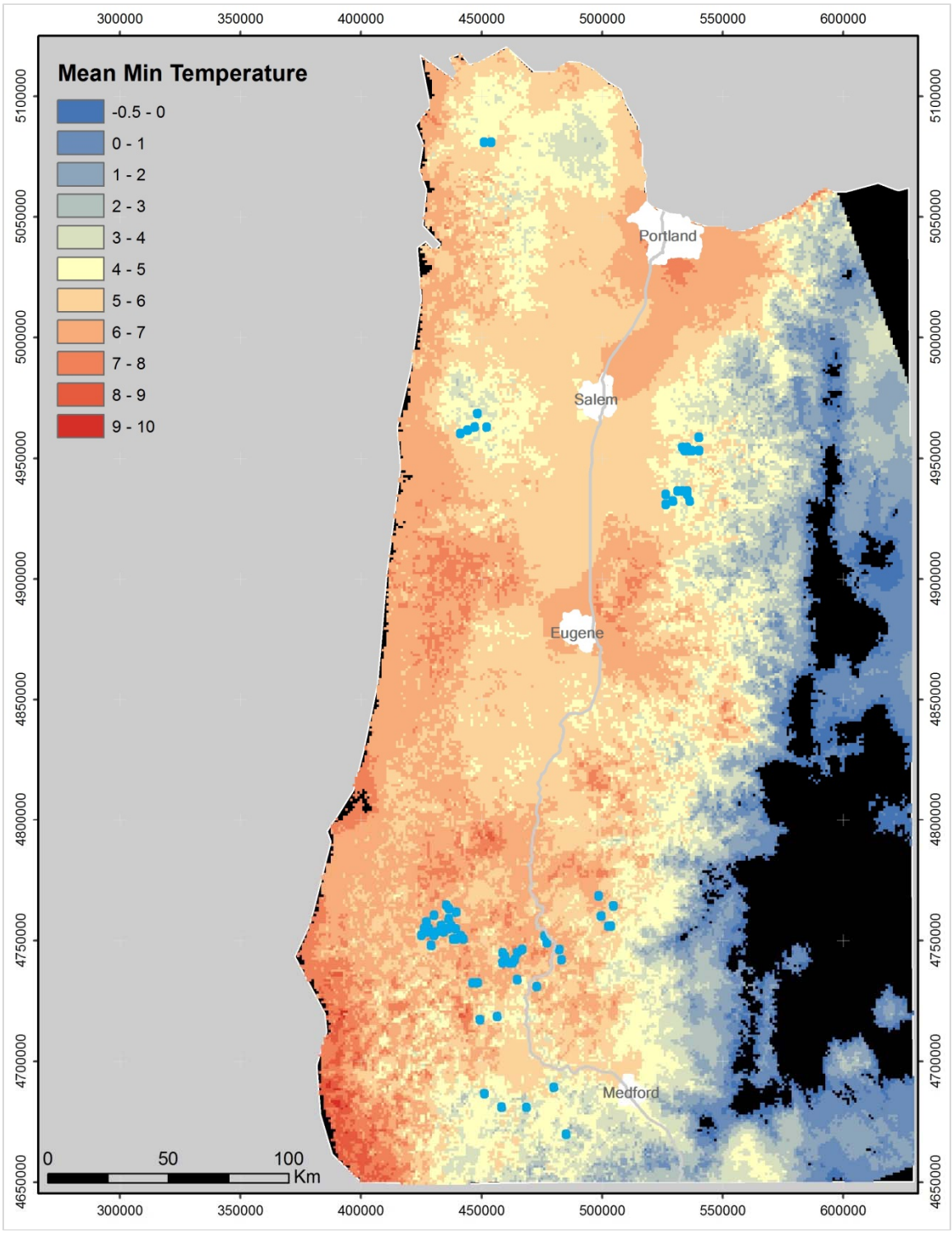

Figure5. Map of mean annual minimum temperatures for western Oregon showing stand locations as blue spots.

LiDAR data

Airborne Laser Scanning (LiDAR) data were acquired from the Oregon Department of Geology and Mineral Industries (DOGAMI). The institution was instrumental in forming the Portland Lidar Consortium, a collaboration that brought together 17 agencies ranging from national agencies to municipalities to acquire 5500 km^2 of public domain observations. This dataset consists out of numerous acquisitions by various vendors and was acquired over multiple years, providing coverage for the majority of forested areas in western Oregon (http://www.oregongeology.org/sub/projects/olc/) (Table 2).

Table 2. LiDAR information for each DOGAMI delivery corresponding to stand locations.

DOGAMI Delivery	Location	Acquisition Date	Avg Point Density/sq meter	Survey Altitute	Pulse Rate
OLC YAMBO	Central Coast Range	2010	9.4	900m and 1300m	>105kHz
OLC NORTH COAST	North Coast	2009	8.5	N/A	N/A
OLC CENTRAL COAST	Central Coast Range	2012	11.5	900m and 1400m	>105kHz
OLC GREEN PETER	West Cascades	2012	9.8	900m	105kHz
OLC SOUTH COAST	South Coast	2008	8.8	N/A	N/A
OLC WILLAMETTE	West Cascades	2009	7.8	N/A	N/A
OLC ROGUE	Klamath Mountains	2012	>8	900m and 1300m	52kHz

Existing LiDAR acquisitions were clipped to the extent of the delineated stands minus a 30m buffer to minimize edge effects and to prevent trees in neighboring stands to affect stand height estimates. Ground returns were identified using FUSION/LDV software (Mc Gaughey, 2007) and a continuous surface model was generated at 1m spatial resolution for each selected stand. To determine stand height we used the surface normalized LiDAR point cloud to run the *CloudMetrics* function in FUSION/LDV. *CloudMetrics* computes a series of descriptive statistics for an input LiDAR dataset including stand heights and height percentiles, a metric that is closely related to height distributions

(Magnussen & Boudewyn, 1998; Naesset, 1997). For the purpose of this study, stand heights were defined as the 95th height percentile of the LiDAR point cloud.

Besides stand heights, we used LiDAR data also to estimate leaf area index (LAI) a parameter that is strongly related to plant growth and soil water balance (McLeod & Running, 1988; Running & Grier, 1977; R.H. Waring, 1983). LiDAR LAI estimation followed methods previously described by several authors (Nicholas C. Coops et al., 2007; Lovell, Jupp, Culvenor, & Coops, 2003; Riaño, Meier, Allgöwer, Chuvieco, & Ustin, 2003). The probability of gap function (Eq. *1*) sums the total number of hits (*#z*) above 2m (*z*) and divides them by the total number of independent hits (*N*):

$$1.\ P_{gap}(z) = 1 - \frac{\{\#z_j | z_j > z\}}{N} \qquad 2.\ L(z) = c(-\log(P_{gap}(z)))$$

The total cumulative foliage area index (LAI) for the height interval from *z* to stand height is given by equation *2*. The value of c is an empirical factor that depends on footprint size, lidar return density and vegetation type under investigation. In order to derive c, we compared the LiDAR estimates of LAI to ground measurements taken by Waring, et al (Pers. Communication) in three different location in the Coast Range. A value of c = 6 was identified in this study.

Growth modeling

Vegetation growth over time and sensitivity of changes in climate were evaluated using a physiological growth model. Different techniques are available. In this study we choose 3PG (Physiological Principles Predicting Growth) is a simplified process-based growth model developed by Landsberg and Waring (1997). The model is optimized for growing conditions in the Pacific North-West of the United States. It predicts stand growth in even aged Douglas-fir plantations but it can be

parameterized for other economically important timber species (Riaño et al., 2003). There are several simplifying assumptions included in the model: 3PG assumes that monthly mean climatic data adequately captures trends in forest growth; NPP and autotrophic respiration are approximately equal fractions of gross photosynthesis across diverse ecosystem types (Landsberg & Sands, 2011; Waring et al., 1998); and that the percentage of NPP allocated to roots increases from 25% to 80% as soil fertility decreases (Landsberg & Waring, 1997). The model estimates the fraction of incoming visible radiation absorbed by the canopy as an exponential function of increasing LAI (Eq. *3*)

3. $\phi_{apar} = 1 - \exp^{(-kLAI)}$

where ϕ_{apar} is the absorbed photosynthetically active radiation (MJ m^{-2} $month^{-1}$), *k* is the light extinction coefficient for conifers (0.5), and *LAI* is the (projected) leaf area index. Predicted LAI and ϕ_{apar} set limits on monthly estimates of gross photosynthesis, canopy evaporation and transpiration, growth allocation, and litter production.

A series of modifiers (*f*) ranging between 0 (complete restriction) to 1 (no restriction) impose restrictions on stomatal conductance, photosynthesis, and transpiration. The combined effect of these modifiers on GPP are expressed through their product as presented in a wide range of equation *4.*

4. $P_G = P_{Eff}\ \phi_{apar}\ f(T)\ f(F)\ f(D)\ f(\Theta_s)\ f(N)\ f(CO_2)$

where P_G is gross photosynthesis (MG C m^{-2} $month^{-1}$), P_{Eff} is photosynthetic light-use efficiency (mol C mol $photon^{-1}$), ϕ_{apar} is the photosynthetically active radiation absorbed by the canopy, *T* represents limitations imposed by deviation from optimum temperature (T_{opt}), *F* is the proportion of days below -2 ^{o}C per month, *D* is daytime vapor pressure deficit constraints in kPa, Θ_s is the restriction

on canopy stomatal conductance (G_c) due to rooting zone soil water deficits, *N* represents nutritional restrictions, and CO_2 refers to the effect of varying atmospheric carbon dioxide (ppm) on P_{Eff} (J. Landsberg & Sands, 2011)

The outputs of the 3-PG model include a number of stand characteristics of interest to ecologists and land managers. The most important outputs are stem density, diameter at breast height (DBH), standing volume, basal area, LAI, NPP, GPP and transpiration, (Landsberg & Waring, 1997).

Model Parameterization

The model was parameterized for Douglas-fir using previously published parameters (Coops, Gaulton, & Waring, 2011; Waring & McDowell, 2002;Waring, Coops, & Running, 2011) (Table 3). Previous studies on forest sites west of the Oregon Cascades have shown an inverse relationship between soil fertility and available soil water. Sites with favorable temperatures and reliable water supply throughout the growing season show greater sensitivity to nutritional limitations whereas nutritional constrains are more likely to affect growth on sites with higher vapor pressure deficits, freezing temperatures, and summer drought(Runyon et al., 1994). For this reason we parameterized 3-PG with maximum ASW offset at 300mm, which proved to be sufficient in most cases to prevent drought-imposed restrictions on GPP throughout the growing season (Waring et al., 2008; Coops et al. 2012).

To assess the soil fertility rating (FR) at each stand, we inverted the 3PG model using a multiple forward mode technique similar to Peddle *et al.*, (2004), by adjusting FR in increments of 0.05, starting at 0.1, until the simulated LAI came within 0.1 of that recorded at the designated stand age by LiDAR on each stand. Based on previous studies of soil fertility (Waring & Youngberg, 1972), it would be

unreasonable to assume that low fertility would be able support the leaf densities observed in this study. For this reason soil fertility values during model inversion were not allowed to take values below 0.1 .

Table 3. 3PG parameters used in this study.

Variable	Functions and parameter values	Source
Max fraction of NPP to roots	0.8	Landsberg & Waring (1997)
Max litter fall rate (1/mo)	2% per month	Landsberg & Waring (1997)
Temperatue limits on light conversion	Tmin=2°C Topt=18°C Tmax=40°C	Landsberg & Waring (1997)
Production day lost per frost	1	
Canopy quantum efficiency	0.055 molC/molPAR	Landsberg & Waring (1997)
Ratio NPP/GPP	0.47	Landsberg & Waring (1997)
LAI for max canopy	5	Landsberg & Waring (1997)
Max canopy conductance	0.012m/s	Landsberg & Waring (1997)
Age at canopy cover	15	Landsberg & Waring (1997)
Wood density	300kg/tree	Landsberg & Waring (1997)
Specific leaf area	5.5	Landsberg & Waring (1997)
Stomatal response to VPD	0.05	Landsberg & Waring (1997)
Soil storage capacity (ASW)	300mm	This study
Soil fertility ranking (FR)	Variable	This study
Convertion of solar radiation to PAR (mol/MJ)	2.3	Landsberg & Waring (1997)

RESULTS

Figure 6 demonstrates a visualization of a LiDAR based height model retrieved for one sample plot area (plus surrounding environment for illustration purposes). The figure at the top illustrates tree heights, that is vegetation heights normalized to the ground elevation, the figure at the bottom illustrates a scene including both ground and tree heights as height above GPS ellipsoid. The height levels are illustrated in different colors and shades. In both images, differences in forest structure are easily recognizable, as are landscape features including roads.

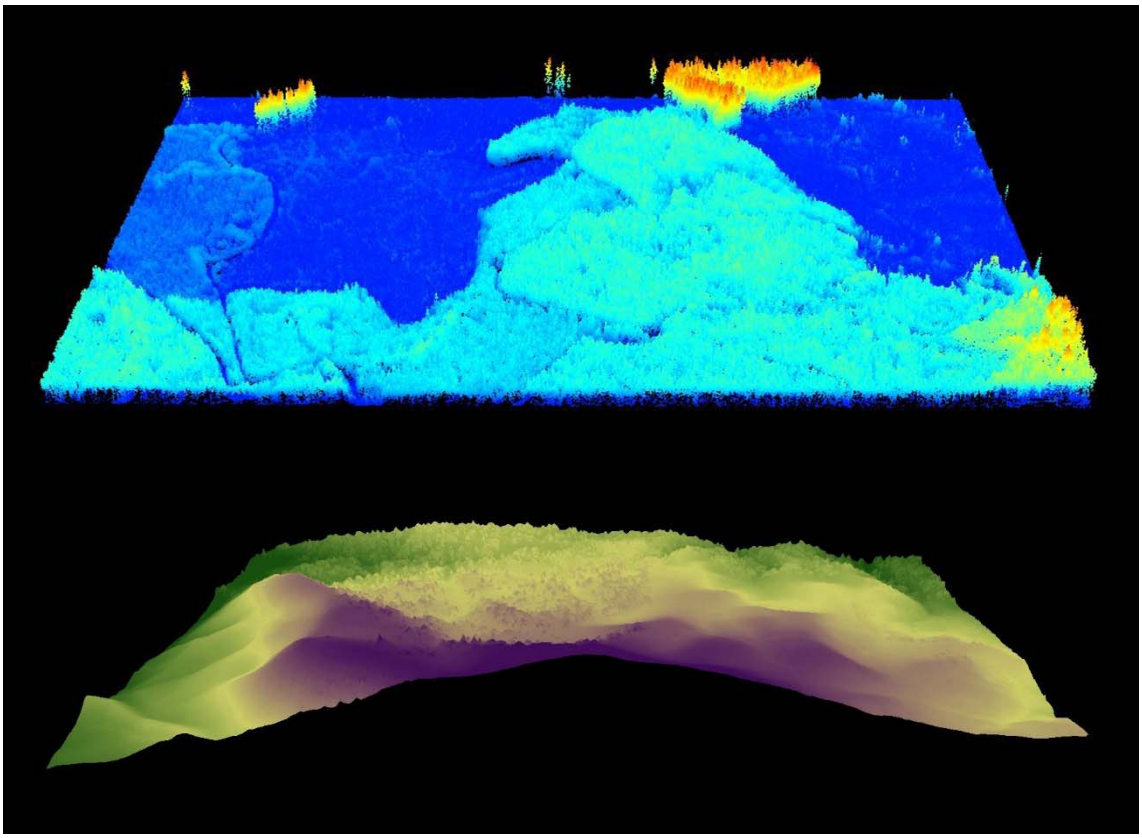

Figure 6. Visualization of surface normalized LiDAR point cloud of different forest in our sampling area. Clear stand delineations, based on height, can be observed on the top image. Dark blue represents ground returns while red represent trees in heights height categories. Image below represent a digital terrain model where dark green represents low elevation and purple represent highest elevation.

Figure 7 shows the Landsat estimated disturbances across western Oregon between 1983 and 2012. The number of disturbances > 1 ha detected with Landsat imagery in the state of Oregon between 1983 and 2012 ranged from< 10,000 to ~1 million ha annually, except in 2002 when the Biscuit Fire (Thompson, Spies, & Ganio, 2007) in southwestern Oregon burnt across 2 million hectares (Figure 7-8). Similarly, total disturbance rates varied between 700 and 1200 km^2 for most years, with the exception of 2002-2003, as a result of the biscuit fire (Thompson et al., 2007) which destroyed large forested areas in south-western Oregon (also visible as green area in the south of the map presented in Figure 7). Also visible in the histogram is the impact of the economic crisis in 2008. During "normal" years, disturbances presented can mostly be interpreted as the result of harvesting activities across the Coast Range and the parts of the Cascades, as well as naturally occurring fires. It should be noted in Figure 8 that the Landsat record utilized in this study started only in 1984. As a result, disturbances detected during the first years, may not be as reliable and should be interpreted with care, as limited visibility due to cloud cover may have prevented a clear view of "baseline" disturbances at the beginning of the time series.

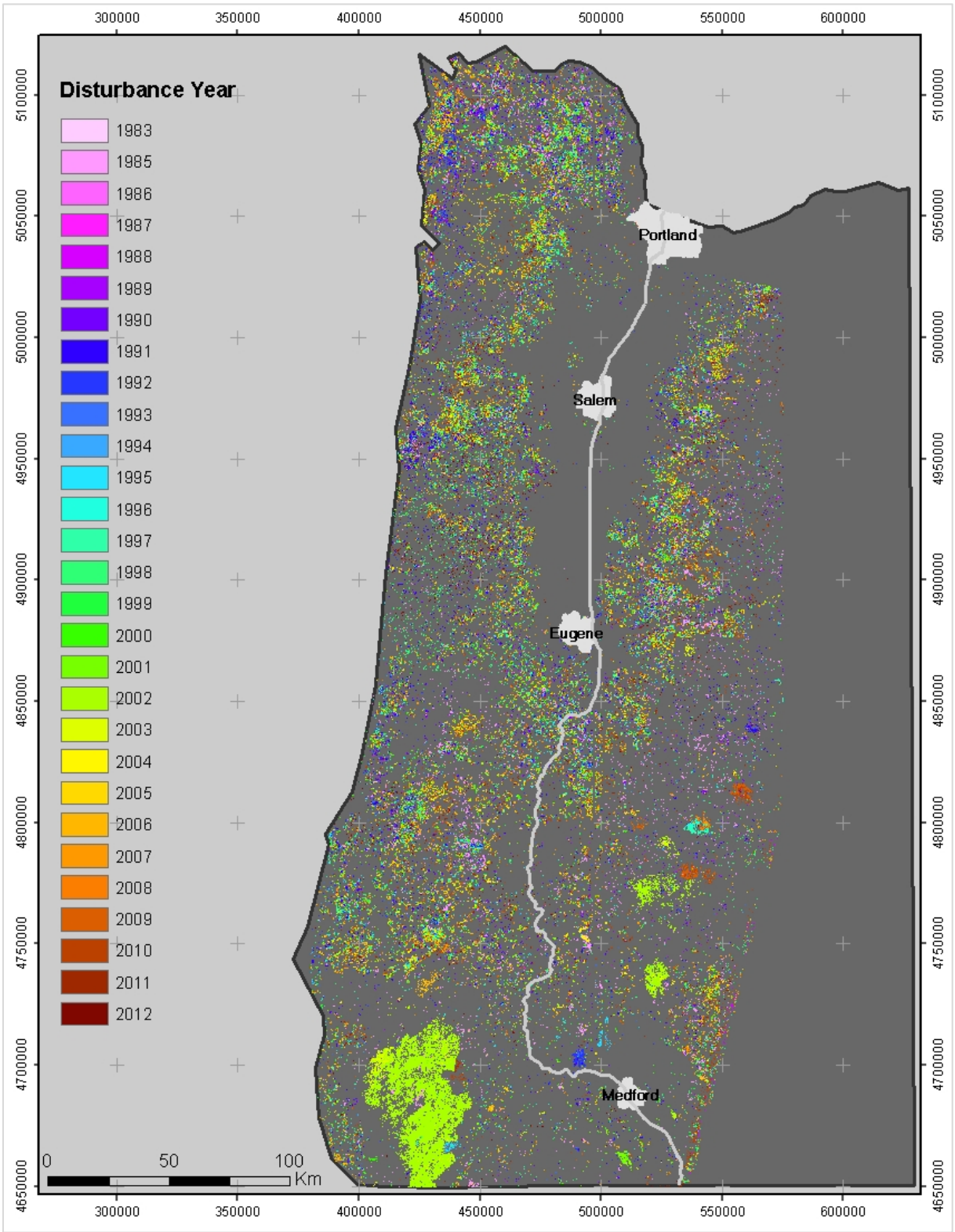

Figure 7. Landsat-derived map of perceived disturbances from 1983-2012 in western Oregon.

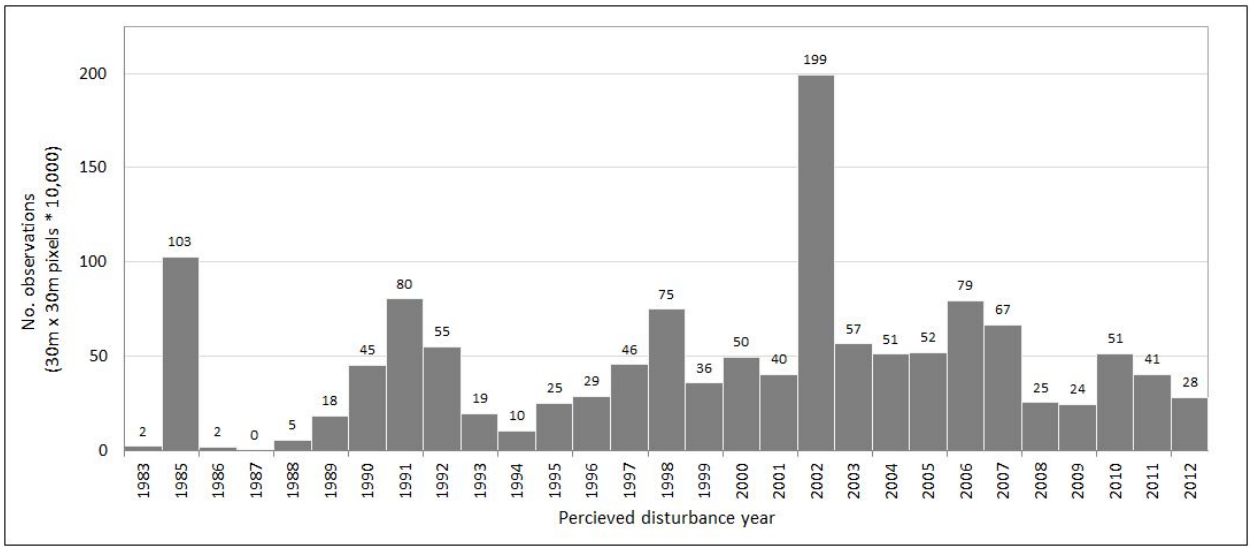

Figure 8. Number of recorded 30x30m disturbances by year in the state of Oregon. Bars represent number of observations on 30x30 meter pixels * 10,000.

Our goal to derive values of FR that resulted in a close match of simulated LAI with those assessed with LiDAR (r^2 = 0.91) were met (Figure 9). LiDAR estimates of LAI ranged between 0.5 and 9.7 . While the relationship of predicted vs observed LAI was near perfect for stands in site class 2, there was somewhat less agreement on S3 and S4. On sites where the LiDAR-derived estimates of LAI were below 3, the 3-PG model overestimated LAI value. This is particularly apparent in S4 stands which showed the most departure from the expected 1:1 relationship between predicted vs observed values.

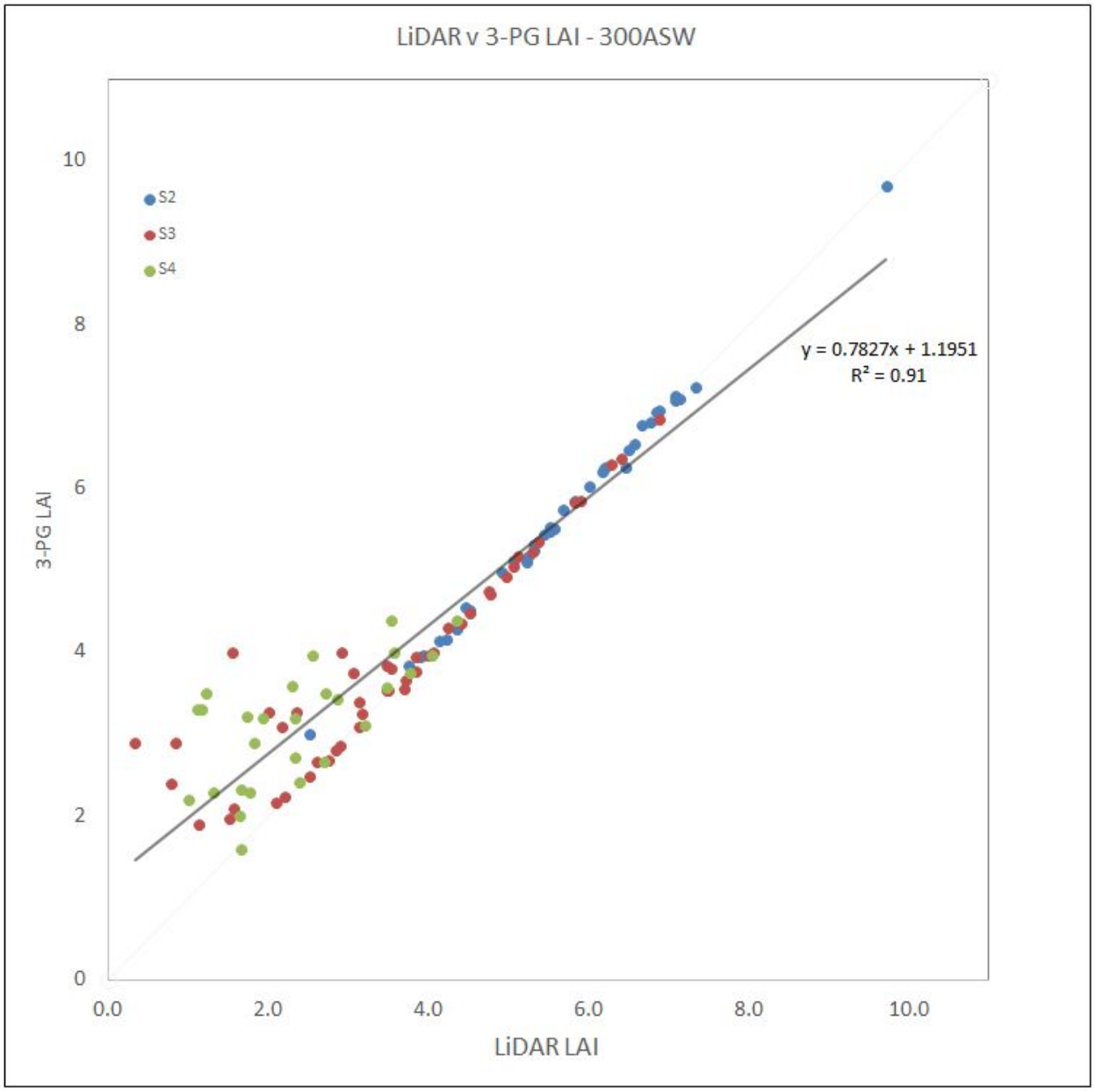

Figure 9. Relationship between 3PG modeled v. LiDAR- derived estimates of LAI. Colors differentiate site classes with blue, red, and green representing S2, S3, and S4 respectively.

The area sampled for S2 and S3 stands both encompassed more than 400 ha, whereas that for S4 stand area totaled only 223 ha (Table 4). The sampling on S2 and S3 stands also included a larger

range in size than S4. The smaller area sampled in S4 reflects our decision to avoid very young stands; as a result, the majority of stands contained trees of older age classes.

Table 4. Sampling statistics of selected forest stands by site class.

	Count	Mean (ha)	Min (ha)	Max (ha)	Sum (ha)
S2	37	11.1	1.1	34.2	412.2
S3	47	11.4	1.5	40.6	539.4
S4	27	8.2	2.2	24.5	223.3
				Total all stands	**1174.9**

Although no direct ground validation of estimated LIDAR stand heights was available, we assumed that LiDAR provided measurement accuracies in the range of previously published literature (about 1.5m) (Naesset, 1997). Both of these assumptions will be discussed in more detail subsequently, but appear to apply generally, and particularly for the highest site class where a linear relation between estimated age and tree height accounts for 61% of the recorded variation. The limits to measuring height with LIDAR probably account, in part, for the reduced correlation on less productive sites (Figure 10).

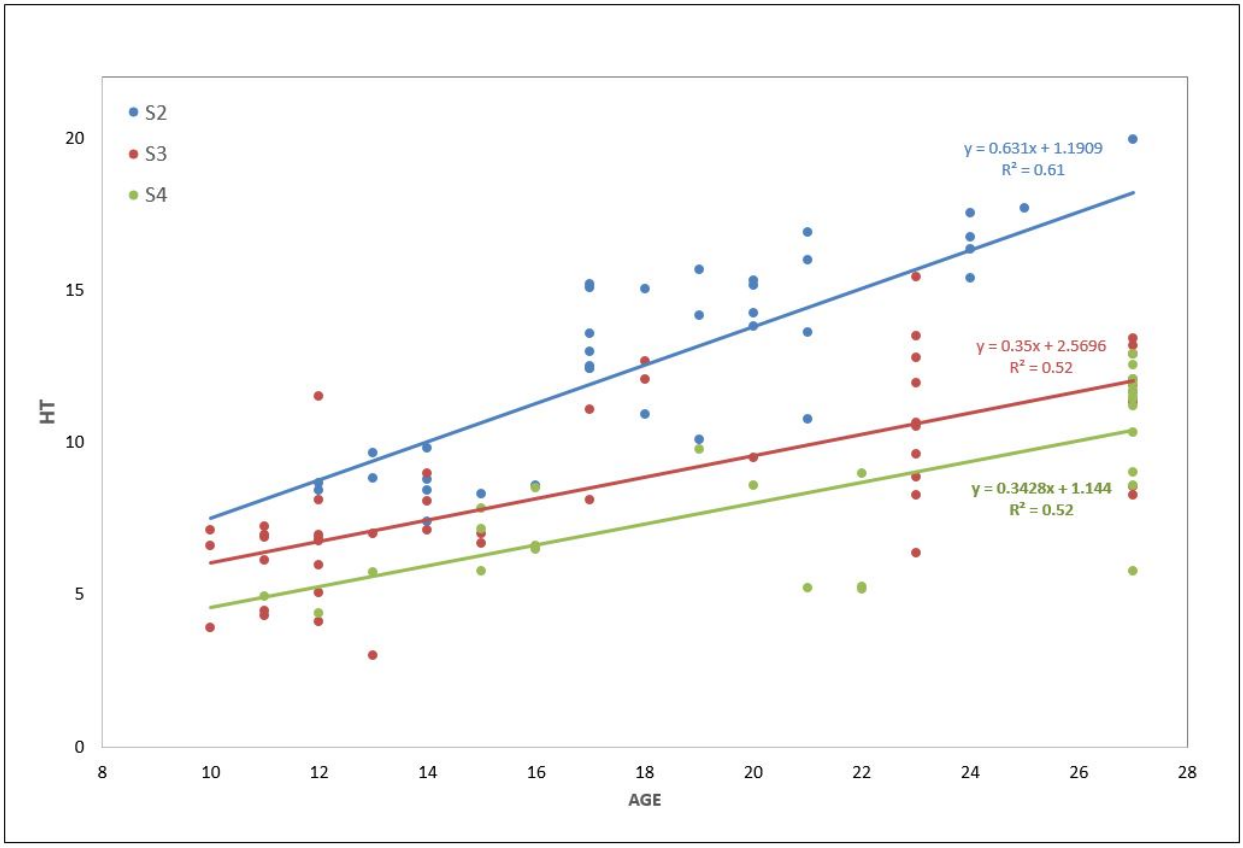

Figure 10. Derived age-height relationship for 111 stands sampled. Height was estimated using the 95th percentile of LiDAR returns, and age was determined as the number of years since disturbance assessed with sequential sets of Landsat imagery.

Estimates of soil fertility ranking (FR) derived by inverting the 3-PG model to match LiDAR-derived LAI, showed progressively less variation and lower mean values going from the most productive to least productive sites (Figure 11). The largest mean and standard deviation variation in FR were recorded at the highest site class (S2) ($\bar{x}$= 0.23, SD ± 0.1) and the least in the lowest (S4) ($\bar{x}$= 0.1, SD ± 0.01). The maximum FR derived for the S2, S3, and S4 were 0.5, 0.4, respectively. No value of FR < 0.1 was permitted in this analysis.

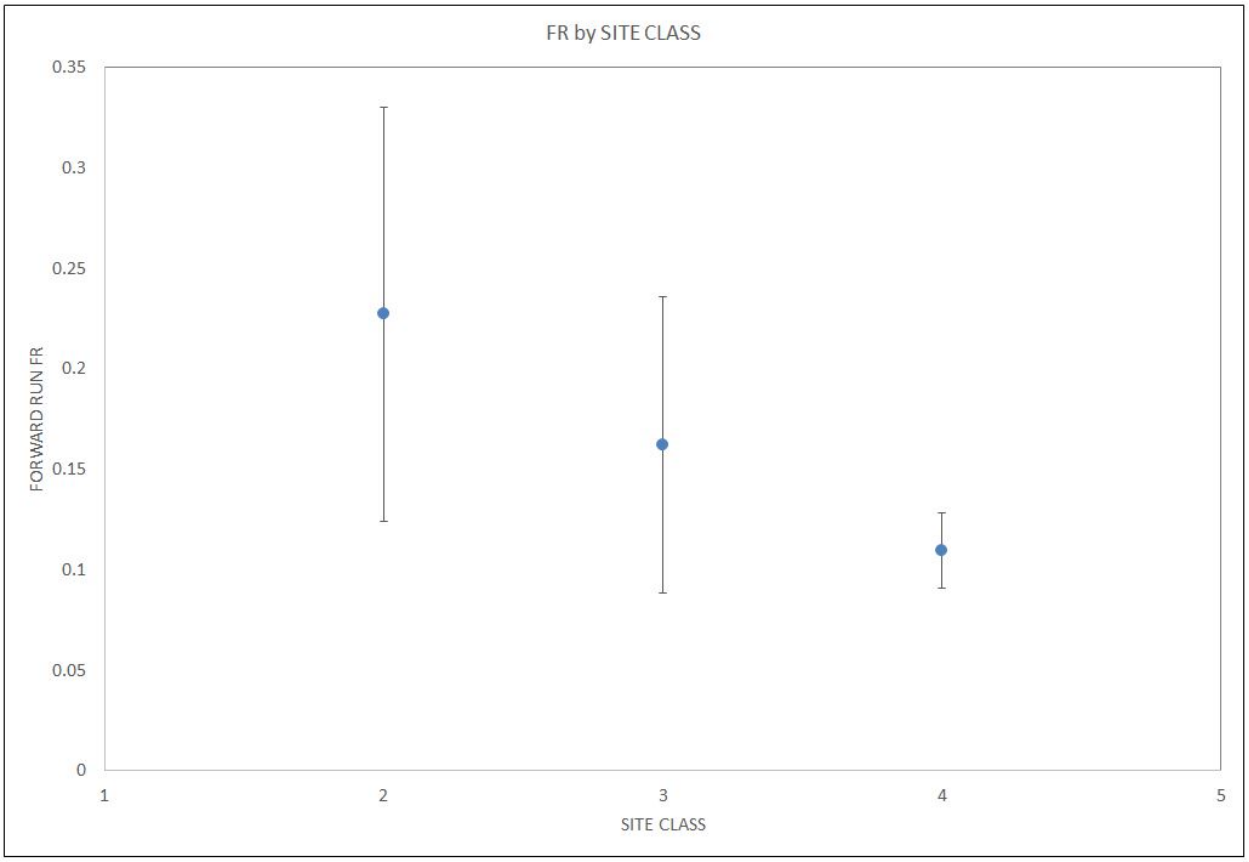

Figure11. Derived soil fertility rankings (FR) from inverting the 3-PG model while assuming that the available soil water storage capacity was fixed at 300mm and that stand leaf area index (LAI) was equivalent to that estimated by LIDAR.

Observed LAI values at the better site class categories stands were consistently higher than those recorded at the next lowest site class category albeit the large variations observed in some age classes for S2 and S3 stands (Figure 12). Although the strength of these relationships were weak (S2, r^2 = 0.15, S3, r^2 = 0.26, and S4, r^2 = 0.17), the expected trend of greater LAI at better site class categories was observed, a result consistent with previous observations of LAI on a productivity gradient (Runyon et al., 1994).

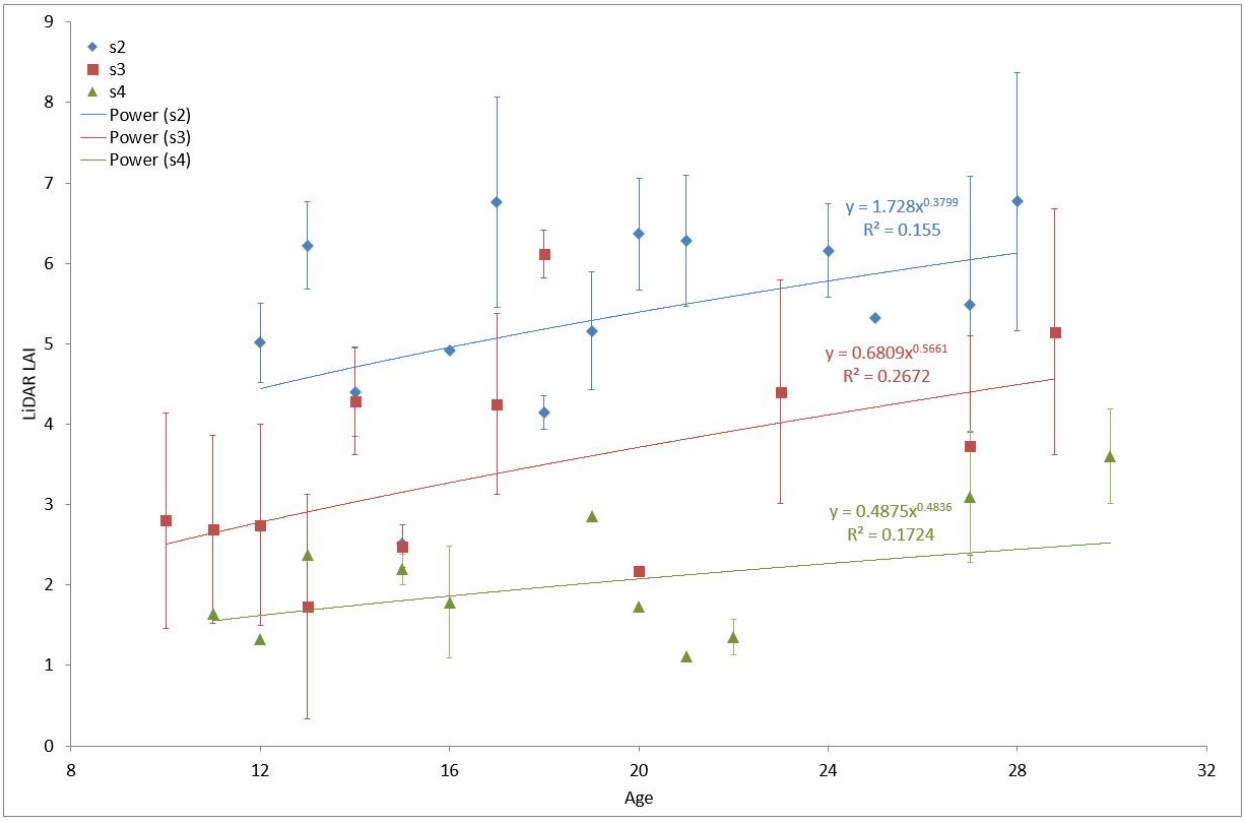

Figure 12. Observed LiDAR LAI plotted against estimated stand age using McArdle *et al.*, (1949) lower to upper height limits for each site class. Error bars represent standard deviations.

DISCUSSION

We used single-flight coverage by LiDAR in combination with sequential annual Landsat composites to assess the ages and heights of 111 Douglas-fir plantations, as well as their leaf area indices. With LAI serving as a reference, we estimated values of soil fertility, derived with a process-based growth model driven with WNA –derived climatic data. Although some of the stands selected contained trees of more than one age class, our LiDAR analysis sought to exclude those not representing the dominant age class. Sometimes harvesting activities appeared to follow fire-induced mortality,

particularly on site class 4. As a result, more errors in the estimation of stand age are likely on the less productive sites, for which fewer samples were also acquired.

Landsat-derived stand ages combined with LiDAR measures of heights allowed us to estimate site indices from age and stand height. Because our sampling precluded ground-based estimates of stand height and ages, we used published height -age relationships from forestry yield tables to assign stands to different site classes. The best results were obtained on the most productive sites, that the maximum annual height growth on these sites come close to the accuracy of LiDAR, ± 1.5m (Naesset, 1997). The high variability in heights within all site classes may indicate artifacts associated with our sampling design. We assumed that differences in LiDAR point densities would not affect estimates of stand heights in fixed area cells and that the associated quantile estimator reflected the true height value for each cell. LiDAR point density is cited as an important aspect for stand height estimation since the probability of hitting the highest point in grid cell decreases when LiDAR point densities are low (Magnussen & Boudewyn, 1998).

By assuming that soil water storage capacity was 300 mm, drought effects were not expressed in this analysis. It was, therefore, a simple process to adjust FR to closely match the LiDAR estimates of LAI. Although we expected higher FR values on all site classes based on bioassays of soils in southwestern Oregon (Waring & Youngberg, 1972), the general trend of higher FR values with improving site classes was observed (Figure 9). Previous attempts to derive soil fertility by inverting the 3-PG model produced estimates of soil fertility in the coast range >0.5 (Coops et al., 2012). The lack of agreement between predicted vs. observed estimates of LAI at the low ranges of LAI in site classes 3 and 4 are likely, at least partially, the result of excluding values of FR generated below 0.1.

Based on a comparison with other climate data sources, we found that WNA point-source data generated larger temperature extremes than those derived from the PRISM model in our study area, which results in higher values in calculated incident radiation (Coops, Waring, & Moncrieff, 2000) and predicted GPP than reported at a number of field sites across western Oregon, as well as measured incident radiation (Runyon et al. 1994). Differences in projected monthly temperature extremes may account for more than 90% of the variation in solar radiation generated by climate models (Coops et al., 2000) (See Appendix A), and selecting lower values would result in increasing the derived estimates of FR. Estimates of monthly precipitation also varied, but were generally sufficient to not create drought conditions with maximum ASW set at 300 mm.

While LiDAR remote sensing is able to provide independent estimates of LAI for forest stands excluding understory vegetation, we expected stronger relationships between stand age and LAI within each site class. Previous studies have found weak relationships when comparing age and LAI (Bryars et al., 2013) due to variation in microclimatic conditions, as well as the effect of competition between young trees and other vegetation. The 3PG model provided estimates of the maximum LAI given a stable climate; it does, however, not account for competition. On the other hand, at intensively managed plantations, competition is minimized so that maximum LAI for any site class may be achieved before age 15 years (Waring, pers. communication). In contrast, the yield tables (McArdle et al., 1961), from which site indices were derived, are based on measurements from stands that established naturally following disturbance.

Misclassification of mapped site classes may also account for some variation in the observed pattern of height growth with age. We assumed mid-point site classes in our analysis, but upper and lower limits of height overlap with adjacent classes in McArdle et al. (1961) (Figure 13). A difference of two meters in height at a given age is often sufficient to shift the classification of a stand to a lower or

higher class. While changing the site classification of some stands may improve the relationship between LAI and age (Figure 14) unaccounted for factors may have affected LAI estimation and weakened the expected relationships among site classes. Because we were limited to areas with LiDAR coverage the distance between our estimated site classes may not have been appropriate to make a clear differentiations. Obviously, the best solution would be to acquire consecutive LiDAR coverage at all sites, and thereby determine actual height growth over a known interval. In addition, stand height heterogeneity may have played a considerable role in assigning LAI values to forest stands. For instance inaccuracies in assigned stand boundaries would allow trees of different height classes to be assigned to the same stand. Future efforts to select even aged forest stand should concentrate on stand height homogeneity if correct LAI estimation is desired.

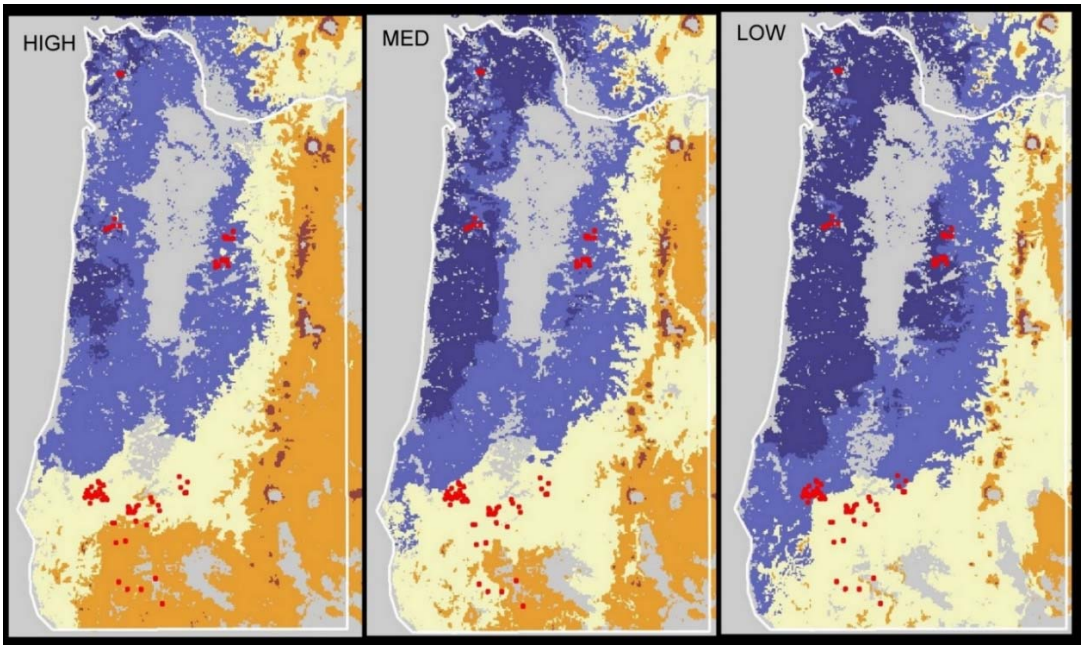

Figure 13. Site index classification in western Oregon using McArdle *et al.*, (1949) yield tables. Red markers represent stand locations. Areas are classified using the lower, mid, and upper limits of height at age 50 which differ from the mid values by 5-7% in height. . Dark blue, light blue, yellow, orange represent S1, S2, S3, S4 respectively.

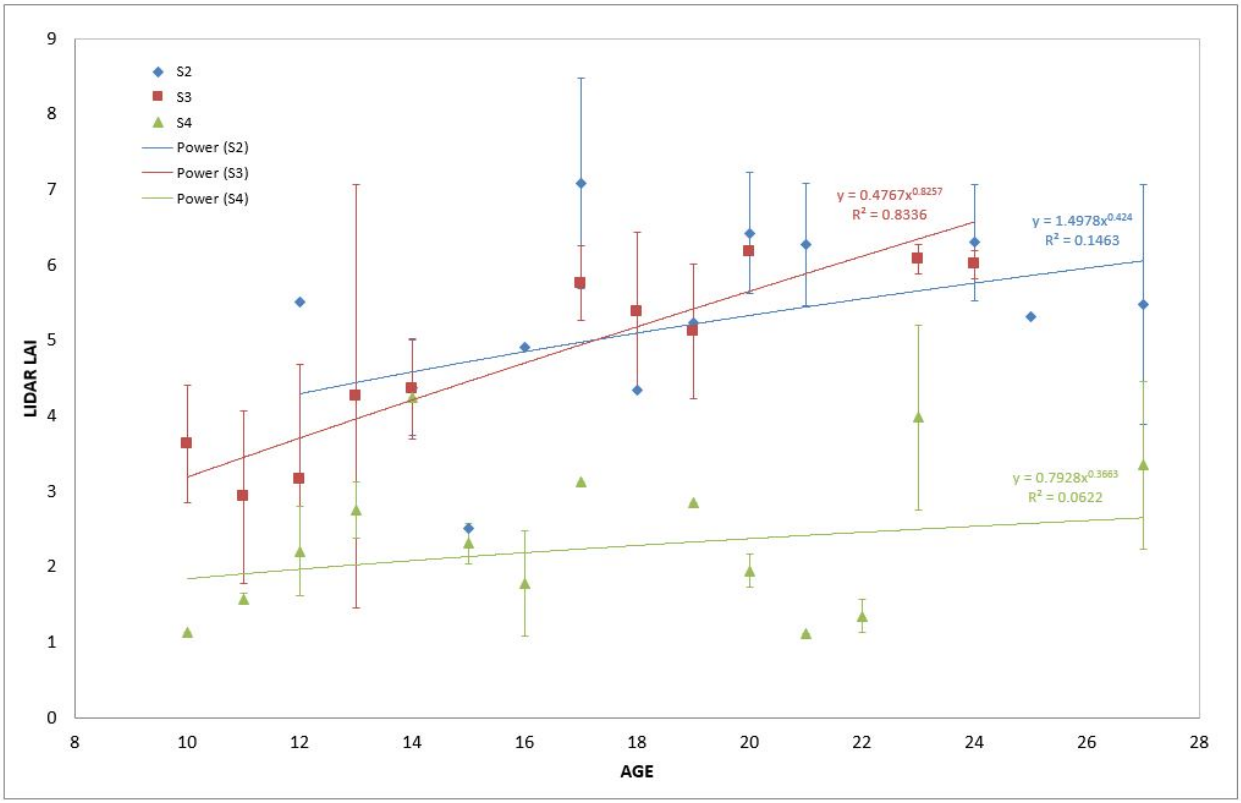

Figure 14. LiDAR LAI v age using the lower limit of the next higher site class height category as the upper limit of the lower site class. By eliminating the 2 meter height gap between site classes it may be possible to improve the relationship between LAI and age. Error bars represent standard deviations.

The derived relationship between LiDAR and 3-PG estimates of LAI suggests that once canopies have closed, this variable alone is a useful index of productivity. Part of the reason for the lack of strong relationships between fertility rate and SI may be incompatibilities of measurements and definitions. For instance the approach used in this paper provides an indirect way to derive soil properties that are otherwise difficult to quantify for deeply rooted trees occupying landscapes with well-developed soil horizons. Once space-borne LiDAR is available, repeat coverage will become more widely available, but challenges will remain in scaling height and LAI measurements across landscapes.

Other factors which may have limited the accuracy of our results include using errors in climate data such as mean monthly solar radiation estimates daily minimum and maximum temperatures. For instance, we found considerable variations in solar radiation estimates as compared to those from ground station measurements. Further efforts to estimate growth in Douglas-fir plantations using 3-PG must include a close examination of climate inputs to ensure that soil fertility and growth estimates are consistent with previously published estimates of soil fertility across Oregon.

CONCLUSION

Using single-flight LiDAR coverage and sequential annual Landsat composites to assess both leaf area index and stand ages in combination with a process-based growth model may improve site growth potential estimation across different climatic regions. Although not without challenges driven mainly by limited data availability and variations in vegetation growth unrelated to soil properties our approach represents an improvement on traditional methods of assigning site growth potential in that it more explicitly accounts for climatic effects included in the growth model (here 3PG) . The need for better management approaches to understand effects of climate change on one hand, but also an operational capacity to derive site based growth potential on the other hand, requires modeling approaches that are relatively easy to implement but account for a wide variety of growing and climate scenarios. We believe our approach addresses some of these challenges. Future studies will have to address the effect of different management regimes on forest growth, as well as differences in species distribution. In addition information on age, thinning and brush control histories may further improve estimates of soil fertility and site growth potential.

This study utilized mean leaf area as observed from LiDAR to infer soil fertility rates and therefore stand growth potential. Future research may benefit from the combination of multiple stand parameters, remotely sensed, as well as retrieved from ground observations to allow for improved model parameterization. Furthermore, Forest stands were selected based on stand disturbance date and using aerial photos to exclude disturbances other than clear cuts. While this method is relatively quick and may address the problems associated with disturbance detection of recent fires it cannot detect or exclude stands recently defoliated by insects, or other disturbances. Our study assumed a homogenous stand structure, as one LAI value was assigned per stand. While this approach has the advantage that it allows a more direct comparison to current inventory metrics, heterogeneous vegetation types , such as naturally regenerated stands, or mixed vegetation types may not be measured using a simple approach like the one described. In summary, this study should be interpreted as a demonstration of a possible approach to more accurately define vegetation growth potential, but a technique as demonstrated would have to be more refined to replace or complement conventional inventory methods.

LITERATURE CITED

Almeida, A. C., Landsberg, J. J., Sands, P. J., Ambrogi, M. S., Fonseca, S., Barddal, S. M., & Bertolucci, F. L. (2004). Needs and opportunities for using a process-based productivity model as a practical tool in Eucalyptus plantations. *Forest Ecology and Management*, *193*(1-2), 167–177. doi:10.1016/j.foreco.2004.01.044

Battaglia, M., & Sands, P. J. (1998). Process-based forest productivity models and their application in forest management. *Forest Ecology and Management*, *102*(1), 13–32. doi:10.1016/S0378-1127(97)00112-6

Bryars, C., Maier, C., Zhao, D., Kane, M., Borders, B., Will, R., & Teskey, R. (2013). Fixed physiological parameters in the 3-PG model produced accurate estimates of loblolly pine growth on sites in different geographic regions. *Forest Ecology and Management*, *289*, 501–514. doi:10.1016/j.foreco.2012.09.031

Constable, J. V. ., & Friend, A. . (2000). Suitability of process-based tree growth models for addressing tree response to climate change. *Environmental Pollution*, *110*(1), 47–59. doi:10.1016/S0269-7491(99)00289-4

Coops, N. C., Gaulton, R., & Waring, R. H. (2011). Mapping site indices for five Pacific Northwest conifers using a physiologically based model. *Applied Vegetation Science*, *14*(2), 268–276. doi:10.1111/j.1654-109X.2010.01109.x

Coops, N. C., Hilker, T., Wulder, M. A., St-Onge, B., Newnham, G., Siggins, A., & Trofymow, J. A. (Tony). (2007). Estimating canopy structure of Douglas-fir forest stands from discrete-return LiDAR. *Trees*, *21*(3), 295–310. doi:10.1007/s00468-006-0119-6

Coops, N. C., & Waring, R. H. (2001a). Estimating forest productivity in the eastern Siskiyou Mountains of southwestern Oregon using a satellite driven process model, 3-PGS. *Canadian Journal of Forest Research*, *31*(1), 143–154. doi:10.1139/cjfr-31-1-143

Coops, N. C., & Waring, R. H. (2001b). The use of multiscale remote sensing imagery to derive regional estimates of forest growth capacity using 3-PGS. *Remote Sensing of Environment*, *75*(3), 324–334. doi:10.1016/S0034-4257(00)00176-0

Coops, N. C., Waring, R. H., & Hilker, T. (2012). Prediction of soil properties using a process-based forest growth model to match satellite-derived estimates of leaf area index. *Remote Sensing of Environment*, *126*, 160–173. doi:10.1016/j.rse.2012.08.024

Coops, N. C., Waring, R. H., & Moncrieff, J. B. (2000). Estimating mean monthly incident solar radiation on horizontal and inclined slopes from mean monthly temperatures extremes. *International Journal of Biometeorology*, *44*(4), 204–211. doi:10.1007/s004840000073

Dubayah, R. O., Sheldon, S. L., Clark, D. B., Hofton, M. A., Blair, J. B., Hurtt, G. C., & Chazdon, R. L. (2010).

Estimation of tropical forest height and biomass dynamics using lidar remote sensing at La Selva, Costa Rica. *Journal of Geophysical Research*, *115*, G00E09. doi:10.1029/2009JG000933

Falkowski, M. J., Hudak, A. T., Crookston, N. L., Gessler, P. E., Uebler, E. H., & Smith, A. M. S. (2010). Landscape-scale parameterization of a tree-level forest growth model: a k- nearest neighbor imputation approach incorporating LiDAR data. *Canadian Journal of Forest Research*, *40*(2), 184–199. doi:10.1139/X09-183

FAO. (2015). *Global Forest Resources Assessment 2015*. Retrieved from http://www.fao.org/forestry/fra2005/en/

Field, C. B., Randerson, J. T., & Malmström, C. M. (1995a). Global net primary production: Combining ecology and remote sensing. *Remote Sensing of Environment*, *51*(1), 74–88. doi:10.1016/0034-4257(94)00066-V

Field, C. B., Randerson, J. T., & Malmström, C. M. (1995b). Global net primary production: Combining ecology and remote sensing. *Remote Sensing of Environment*, *51*(1), 74–88. doi:10.1016/0034-4257(94)00066-V

Ford, E. D., & Bassow, S. L. (1989). Modeling the dependence of forest growth on environmental influences. In *Biomass Production by Fast-Growing Trees* (pp. 209–229). Springer.

Franklin, J. F., & Dyrness, C. T. (1988). *Natural vegetation of Oregon and Washington*. Corvallis: Oregon State University Press.

Fu, P., & Rich, P. M. (2002). A geometric solar radiation model with applications in agriculture and forestry. *Computers and Electronics in Agriculture*, *37*(1-3), 25–35. doi:10.1016/S0168-1699(02)00115-1

Gibbs, H. K., Brown, S., Niles, J. O., & Foley, J. A. (2007). Monitoring and estimating tropical forest carbon stocks: making REDD a reality. *Environmental Research Letters*, *2*(4), 045023. doi:10.1088/1748-9326/2/4/045023

Goetz, S. J., Prince, D., Goward, N., Thawley, M. M., Small, J., & Johnston, A. (1999). Mapping net primary production and related biophysical variables with remote sensing: Application to the BOREAS region. *Journal of Geophysical Research*, *104*, 27719–27734.

Harkonen, S., Tokola, T., Packlen, P., Korhonen, L., & Makela, A. (2013). Predicting forest growth based on airborne light detection and ranging data , climate data , and a simplified process-based model. *Canadian Journal of Forest Research*, *43*, 364–375.

Hilker, T., Coops, N. C., Hall, F. G., Black, T. A., Chen, B., Krishnan, P., … Huemmrich, K. F. (2008). A modeling approach for upscaling gross ecosystem production to the landscape scale using remote sensing data. *Journal of Geophysical Research*, *113*(G3), G03006. doi:10.1029/2007JG000666

Imhoff, M., Story, M., Vermillion, C., Khan, F., & Polcyn, F. (1986). Forest canopy characterization and

vegetation penetration assessment with space-borne radar. *Geoscience and Remote Sensing, IEEE Transactions on*, (4), 535–542.

Jarvis, P. G., & Leverenz, J. W. (1983). Productivity of temperate, deciduous and evergreen forests. In *Physiological plant ecology IV* (pp. 233–280). Springer.

Kimball, J. S., Running, S. W., & Nemani, R. (1997). An improved method for estimating surface humidity from daily minimum temperature. *Agricultural and Forest Meteorology*, *85*(1-2), 87–98. doi:10.1016/S0168-1923(96)02366-0

Kira, T., & Shidei, T. (1967). Primary production and turnover of organic matter in different forest ecosystems of the western pacific. *Japanese Journal of Ecology*, *17*(2), 70–87. Retrieved from http://ci.nii.ac.jp/naid/110001882793/en/

Koetz, B., Sun, G., Morsdorf, F., Ranson, K. J., Kneubühler, M., Itten, K., & Allgöwer, B. (2007). Fusion of imaging spectrometer and LIDAR data over combined radiative transfer models for forest canopy characterization. *Remote Sensing of Environment*, *106*(4), 449–459. doi:10.1016/j.rse.2006.09.013

Kohl, M., Lasco, R., Cifuentes, M., Jonsson, O., Korhonen, K. T., Mundhenk, P., … Stinson, G. (2015). Changes in forest production, biomass and casbon: result from the 2015 UN FAO Global Forest Resource Assessment. *Forest Ecology and Management*, *352*, 21–34. doi:10.1016/j.foreco.2015.05.036

Korhonen, L., Korpela, I., Heiskanen, J., & Maltamo, M. (2011). Airborne discrete-return LIDAR data in the estimation of vertical canopy cover, angular canopy closure and leaf area index. *Remote Sensing of Environment*, *115*(4), 1065–1080. doi:10.1016/j.rse.2010.12.011

Landgrebe, D. (1997). The Evolution of Landsat Data. *Photogrammetric Engineering & Remote Sensing*, *63*(7), 859–867. Retrieved from http://citeseerx.ist.psu.edu/viewdoc/download?doi=10.1.1.80.4072&rep=rep1&type=pdf

Landsberg, J. J., & Waring, R. H. (1997). A generalised model of forest productivity using simplified concepts of radiation use efficiency carbon balance and partitioning. *Forest Ecology and Management*, *95*(3), 209–228. doi:10.1016/S0378-1127(97)00026-1

Landsberg, J., & Sands, P. (2011). *Physiolocical Ecology of Forest Production* (First). London: Academic Press.

Latta, G., Temesgen, H., & Barrett, T. M. (2009). Mapping and imputing potential productivity of Pacific Northwest forests using climate variables. *Canadian Journal of Forest Research*, *39*(6), 1197–1207. doi:10.1139/X09-046

Law, B. E., & Waring, R. H. (2015). Carbon implications of current and future effects of drought, fire and management on Pacific Northwest forests. *Forest Ecology and Management*, *355*, 4–14.

doi:10.1016/j.foreco.2014.11.023

Lefsky, M. A., Harding, D. J., Keller, M., Cohen, W. B., Carabajal, C. C., Del Bom Espirito-Santo, F., … de Oliveira, R. (2005). Estimates of forest canopy height and aboveground biomass using ICESat. *Geophysical Research Letters*, *32*(22), L22S02. doi:10.1029/2005GL023971

Lefsky, M. A., Turner, D. P., Guzy, M., & Cohen, W. B. (2005). Combining lidar estimates of aboveground biomass and Landsat estimates of stand age for spatially extensive validation of modeled forest productivity. *Remote Sensing of Environment*, *95*(4), 549–558. Retrieved from http://www.sciencedirect.com/science/article/pii/S0034425705000258

Lim, K., Treitz, P., Wulder, M., St-Onge, B., & Flood, M. (2003). LiDAR remote sensing of forest structure. *Progress in Physical Geography*, *27*(1), 88–106. doi:10.1191/0309133303pp360ra

Lovell, J. L., Jupp, D. . B., Culvenor, D. S., & Coops, N. C. (2003). Using airborne and ground-based ranging lidar to measure canopy structure in Australian forests. *Canadian Journal of Remote Sensing*, *29*(5), 607–622. doi:10.5589/m03-026

Magnussen, S., & Boudewyn, P. (1998). Derivations of stand heights from airborne laser scanner data with canopy-based quantile estimators. *Canadian Journal of Forest Research*, *28*(7), 1016–1031. doi:10.1139/cjfr-28-7-1016

Masek, J. G., Vermote, E. F., Saleous, N., Wolfe, R., Hall, F. G., Huemmrich, K. F., … Lim, T. K. (2013). LEDAPS Calibration, Reflectance, Atmospheric Correction Preprocessing Code, Version 2. ORNL Distributed Active Archive Center. doi:10.3334/ORNLDAAC/1146

Mc Gaughey, R. J. (2007). FUSION/LDV: software for LIDAR data analysis and visualization. USDA Forest Service. *Pacific Northwest Research Station*, 28–30.

Mcardle, R. E., Meyer, W. H., & Bruce, D. (1949). The Yield of Douglas Fir in the Pacific Northwest. *US Department of Agriculture. Technical Bulleltin No. 201.*, (201), 82. Retrieved from http://naldc.nal.usda.gov/download/CAT40000043/PDF

McLeod, S. D., & Running, S. W. (1988). Comparing site quality indexes and productivity in ponderosa pine stands of western Montana. *Canadian Journal of Forest Research*, *18*, 346–352.

Monserud, R. A., & Rehfeldt, G. E. (1990). Genetic and environmental components of variation of site index in inland Dougls-fir. *Forest Science*, *36*(1), 1–9. doi:S

Monserud, R. A., Yang, Y., Huang, S., & Tchebakova, N. (2008). Potential change in lodgepole pine site index and distribution under climatic change in Alberta. *Canadian Journal of Forest Research*, *38*(2), 343–352. doi:10.1139/X07-166

Moran, M. S., Maas, S. J., & Pinter, P. J. (1995). Combining remote sensing and modeling for estimating surface evaporation and biomass production. *Remote Sensing Reviews*, *12*(3-4), 335–353. doi:10.1080/02757259509532290

Muning, R., Thiaw, I., Thopmson, J., Ganz, D., Girvetz, E., & Rivington, M. (2011). *Sustaining Forests: Investing in our common future*. *UNEP Policy Series - Ecosystem Management*.

Naesset, E. (1997). Determination of mean tree height of forest stands using airborne laser scanner data. *ISPRS Journal of Photogrammetry and Remote Sensing*, *52*(2), 49–56. doi:10.1016/S0924-2716(97)83000-6

Naesset, E., & Okland, T. (2002). Estimating tree height and tree crown properties using airborne scanning laser in a boreal nature reserve. *Remote Sensing of Environment*, *79*(1), 105–115. doi:10.1016/S0034-4257(01)00243-7

Neigh, C. S. R., Masek, J. G., Bourget, P., Rishmawi, K., Zhao, F., Huang, C., … Nelson, R. F. (2016). Regional rates of young US forest growth estimated from annual Landsat disturbance history and IKONOS stereo imagery. *Remote Sensing of Environment*, *173*, 282–293. doi:10.1016/j.rse.2015.09.007

Nemani, R. R., Keeling, C. D., Hashimoto, H., Jolly, W. M., Piper, S. C., Tucker, C. J., … Running, S. W. (2003). Climate-driven increases in global terrestrial net primary production from 1982 to 1999. *Science (New York, N.Y.)*, *300*(5625), 1560–3. doi:10.1126/science.1082750

Pan, S., Tian, H., Dangal, S. R. S., Ouyang, Z., Tao, B., Ren, W., … Running, S. (2014). Modeling and monitoring terrestrial primary production in a changing global environment: Toward a multiscale synthesis of observation and simulation. *Advances in Meteorology*, *2014*.

Peddle, D. R., Johnson, R. L., Cihlar, J., & Latifovic, R. (2004). Large area forest classification and biophysical parameter estimation using the 5-Scale canopy reflectance model in Multiple-Forward-Mode. *Remote Sensing of Environment*, *89*(2), 252–263. doi:10.1016/j.rse.2002.08.001

Persson, A., Holmgren, J., & Söderman, U. (2002). Detecting and measuring individual trees using an airborne laser scanner. *Photogrammetric Engineering and Remote Sensing*, *68*(9), 925–932.

Popescu, S. C., Wynne, R. H., & Nelson, R. F. (2003). Measuring individual tree crown diameter with lidar and assessing its influence on estimating forest volume and biomass. *Canadian Journal of Remote Sensing*, *29*(5), 564–577. doi:10.5589/m03-027

Powell, S. L., Cohen, W. B., Healey, S. P., Kennedy, R. E., Moisen, G. G., Pierce, K. B., & Ohmann, J. L. (2010). Quantification of live aboveground forest biomass dynamics with Landsat time-series and field inventory data: A comparison of empirical modeling approaches. *Remote Sensing of Environment*, *114*(5), 1053–1068. doi:10.1016/j.rse.2009.12.018

Randerson, J. T., Chapin, F. S., Harden, J. W., Neff, J. C., & Harmon, M. E. (2002). Net ecosystem production: A comprehensive measure of net carbon accumulation by ecosystems. *Ecological Applications*, *12*(4), 937–947. doi:10.1890/1051-0761(2002)012[0937:NEPACM]2.0.CO;2

Riaño, D., Meier, E., Allgöwer, B., Chuvieco, E., & Ustin, S. L. (2003). Modeling airborne laser scanning

data for the spatial generation of critical forest parameters in fire behavior modeling. *Remote Sensing of Environment*, *86*(2), 177–186. doi:10.1016/S0034-4257(03)00098-1

Running, S. W. ., & Grier, C. G. . (1977). Leaf Area of Mature Northwestern Coniferous Forests : Relation to Site Water Balance. *Ecology*, *58*(4), 893–899.

Runyon, J., Waring, R. H., Goward, S. N., & Welles, J. M. (1994). Environmental Limits on Net Primary Production and Light-Use Efficiency Across the Oregon Transect. *Ecological Applications*, *4*(2), 226–237.

S. E. Franklin , M. B. Lavigne , M. J. Deuling, M. A. W. & E. R. H. J., Franklin, S. E., Lavigne, M. B., Deuling, M. J., Wulder, M. A., Jr., E. R. H., … Hunt, E. R. (1997). Estimation of forest Leaf Area Index using remote sensing and GIS data for modelling net primary production. *International Journal of Remote Sensing*, *18*(16), 3459–3471. doi:10.1080/014311697216973

Schenk, T., Seo, S., & Csatho, B. (2001). Accuracy study of airborne laser scanning data with photogrammetry. *International Archives of Photogrammetry and Remote Sensing*, *34*(part 3), W4.

Schroeder, T. A., Hember, R., Coops, N. C., & Liang, S. (2009). Validation of Solar Radiation Surfaces from MODIS and Reanalysis Data over Topographically Complex Terrain. *Journal of Applied Meteorology and Climatology*, *48*(12), 2441–2458. doi:10.1175/2009JAMC2152.1

Skovsgaard, J. P., & Vanclay, J. K. (2008). Forest site productivity: a review of the evolution of dendrometric concepts for even-aged stands. *Forestry*, *81*(1), 13–31. doi:10.1093/forestry/cpm041

Steffer, W., Nobel, I., & Canadell, J. (1998). The terrestrial carbon cycle: implication for the Kyoto protocol. *Science*, *280*, 1393–1394.

Thompson, J. R., Spies, T. A., & Ganio, L. M. (2007). Reburn severity in managed and unmanaged vegetation in a large wildfire. *Proceedings of the National Academy of Sciences of the United States of America*, *104*(25), 10743–8. doi:10.1073/pnas.0700229104

Valentine, H. (1997). Height growth, site index, and carbon metabolism. *Silva Fennica*, *31*(3), 251–263. Retrieved from http://helda.helsinki.fi/handle/1975/8524

van Leeuwen, M., & Nieuwenhuis, M. (2010). Retrieval of forest structural parameters using LiDAR remote sensing. *European Journal of Forest Research*, *129*(4), 749–770. doi:10.1007/s10342-010-0381-4

Vermote, E. F., El Saleous, N., Justice, C. O., Kaufman, Y. J., Privette, J. L., Remer, L., … Tanre, D. (1997). Atmospheric correction of visible to middle-infrared EOS-MODIS data over land surfaces: Background, operational algorithm and validation. *NASA Publications*, 31.

Waring, R. H. (1983). Estimating forest growth and efficiency in relation to canopy leaf area. *Advances in Ecological Research*, *13*, 327–354. doi:10.1016/S0065-2504(08)60111-7

Waring, R. H., Coops, N. C., & Landsberg, J. J. (2010). Improving predictions of forest growth using the 3-PGS model with observations made by remote sensing. *Forest Ecology and Management*, *259*(9), 1722–1729. doi:10.1016/j.foreco.2009.05.036

Waring, R. H., Coops, N. C., & Running, S. W. (2011). Predicting satellite-derived patterns of large-scale disturbances in forests of the Pacific Northwest Region in response to recent climatic variation. *Remote Sensing of Environment*, *115*(12), 3554–3566. doi:10.1016/j.rse.2011.08.017

Waring, R. H., Landsberg, J. J., & Williams, M. (1998). Net primary production of forests: a constant fraction of gross primary production? *Tree Physiology*, *18*(2), 129–134. doi:10.1093/treephys/18.2.129

Waring, R. H., & McDowell, N. (2002). Use of a physiological process model with forestry yield tables to set limits on annual carbon balances. *Tree Physiology*, *22*, 179–188.

Waring, R. H., & Youngberg, C. T. (1972). Evalutating forest sites for potential growth response of trees to fertilizer. *Northwest Science*, *46*(1), 67 – 75. Retrieved from http://www.fsl.orst.edu/~waring/Publications/pdf/Waring and Youngberg 1972.pdf

Weiskittel, A. R., Hann, D., Kershaw, J. A. J., & Vanclay, J. K. (2011). *Forest Growth and Yield Modeling*. Somerset, NJ, USA: John Wiley & Sons. Retrieved from http://site.ebrary.com/lib/oregonstate/docDetail.action?docID=10575545

Wulder, M. A., Bater, C. W., Coops, N. C., Hilker, T., & White, J. C. (2008). The role of LiDAR in sustainable forest management. *The Forestry Chronicle*, *84*(6), 807–826. doi:10.5558/tfc84807-6

Wulder, M. A., White, J. C., Nelson, R. F., Næsset, E., Ørka, H. O., Coops, N. C., … Gobakken, T. (2012). Lidar sampling for large-area forest characterization: A review. *Remote Sensing of Environment*, *121*, 196–209. doi:10.1016/j.rse.2012.02.001

Xiaoye Liu. (2008). Airborne LiDAR for DEM generation: some critical issues. *Progress in Physical Geography*, *32*(1), 31–49. doi:10.1177/0309133308089496

Zhu, Z., & Woodcock, C. E. (2012). Object-based cloud and cloud shadow detection in Landsat imagery. *Remote Sensing of Environment*, *118*, 83–94. doi:10.1016/j.rse.2011.10.028

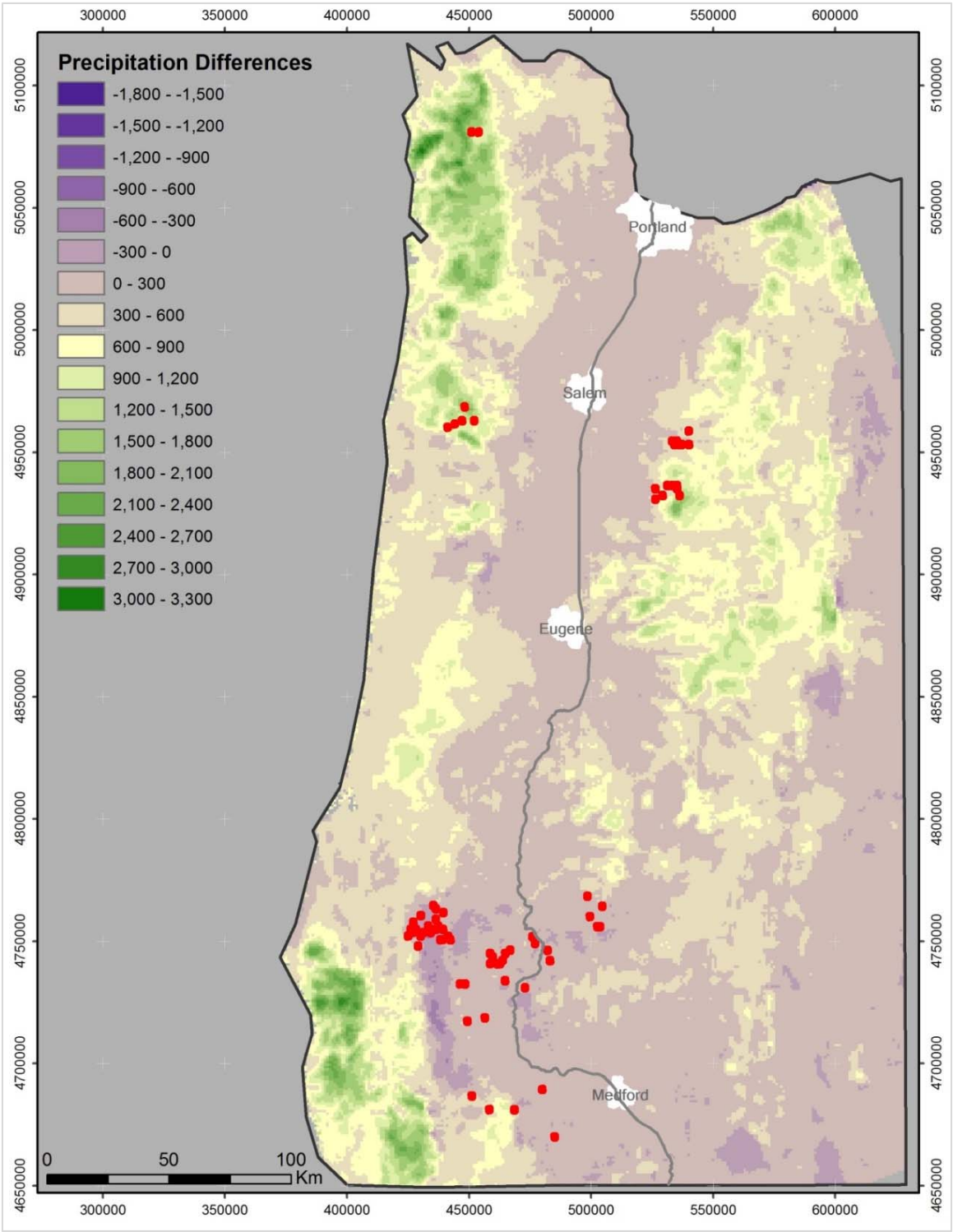

Figure A1. Differences in mean annual precipitation (mm) projected by ClimateWNA in comparison to the PRISM model in western Oregon. Red dots represent stand locations.

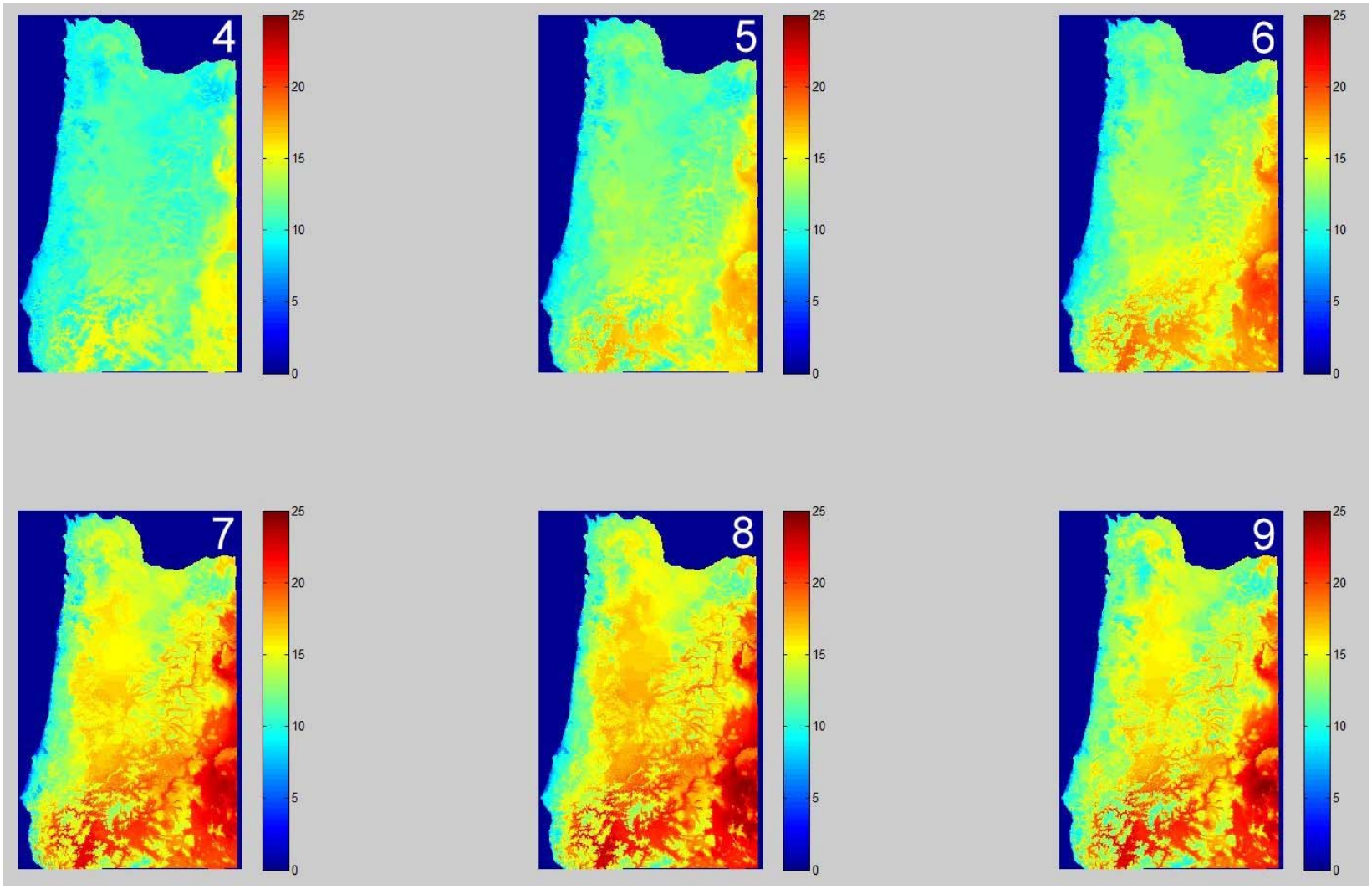

Figure A2. Range in PRISM maximum and minimum temperatures across western Oregon for the months of April (4) to September (9). Temperatures are in ^{o}C.

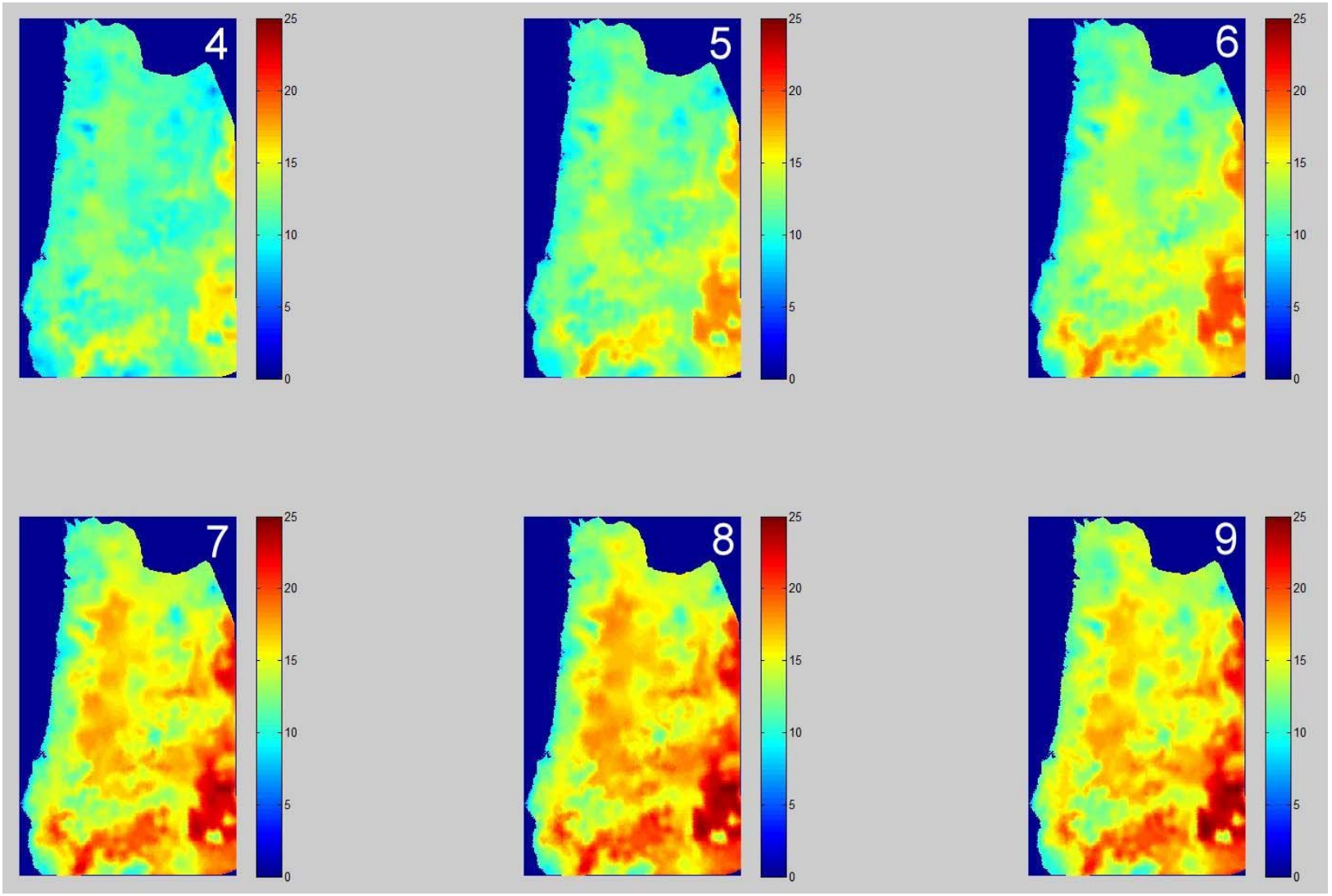

Figure A3. ClimateWNA maximum and minimum temperature ranges for the months of April to September across western Oregon. Temperatures are in ^{o}C.